

ARTICLE

Mechanisms of proton inhibition and sensitization of the cation channel TRPV3

Haiyuan Wang^{1,2} , Pu Yang², Yungang Lu², Jin Wang³, Jaepyo Jeon² , Qiaochu Wang², Jin-Bin Tian², Bin Zang¹, Ye Yu^{3,4}, and Michael X. Zhu² 

TRPV3 is a temperature-sensitive, nonselective cation channel expressed prominently in skin keratinocytes. TRPV3 plays important roles in hair morphogenesis and maintenance of epidermal barrier function. Gain-of-function mutations of TRPV3 have been found in both humans and rodents and are associated with hair loss, pruritus, and dermatitis. Here, we study the mechanisms of acid regulation of TRPV3 by using site-directed mutagenesis, fluorescent intracellular calcium measurement, and whole-cell patch-clamp recording techniques. We show that, whereas extracellular acid inhibits agonist-induced TRPV3 activation through an aspartate residue (D641) in the selectivity filter, intracellular protons sensitize the channel through cytoplasmic C-terminal glutamate and aspartate residues (E682, E689, and D727). Neutralization of the three C-terminal residues presensitizes the channel to agonist stimulation. Molecular dynamic simulations revealed that charge neutralization of the three C-terminal residues stabilized the sensitized channel conformation and enhanced the probability of α -helix formation in the linker between the S6 transmembrane segment and TRP domain. We conclude that acid inhibits TRPV3 function from the extracellular side but facilitates it from the intracellular side. These novel mechanisms of TRPV3 proton sensing can offer new insights into the role of TRPV3 in the regulation of epidermal barrier permeability and skin disorders under conditions of tissue acidosis.

Introduction

TRPV3 is a member of the transient receptor potential vanilloid (TRPV) subfamily of Ca^{2+} -permeable cation channels. It is closely related to TRPV1, the founding member of the TRPVs and well known to function in nociceptive sensory nerves in response to a broad array of painful stimuli, such as noxious heat, acidosis, and inflammatory mediators (Bandell et al., 2007; Latorre et al., 2007; Jara-Oseguera et al., 2008). In mammals, the genes for TRPV1 and TRPV3 exist in tandem on the same chromosome locus with the same transcriptional orientation, indicative of gene duplication; however, TRPV3 is distinct from TRPV1 in that it is mainly expressed in skin keratinocytes and the epithelial lining of the oral cavity (Peier et al., 2002; Xu et al., 2006), and it is activated by innocuous warm temperatures with reported thresholds of 31–39°C (Peier et al., 2002; Smith et al., 2002; Xu et al., 2002), far lower than that needed for the heat-evoked activation of TRPV1 (~42°C; Caterina et al., 1997). The significance of TRPV3 in human health is clearly indicated by the genetic mutations of this channel that underlie Olmsted syndrome (OS), a rare congenital skin disease with clinical features of palmoplantar and periorificial keratoderma, alopecia,

and severe pruritus (Lin et al., 2012; Wilson et al., 2015). Intriguingly, the two most common mutations found in human patients, namely Gly573Ser and Gly573Cys (Lin et al., 2012; Wilson et al., 2015), also exist in the spontaneous hairless mouse and rat strains, *DS-Nh* mouse and *WBN/Kob-Ht*, respectively, and these animals develop dermatitis and itch phenotypes as well (Asakawa et al., 2006; Yoshioka et al., 2009).

Both Gly573Ser and Gly573Cys as well as several other OS-causing mutations of TRPV3 showed high constitutive channel activity when heterologously expressed, indicating that the skin dysfunction is caused by gain of function of the TRPV3 channel (Xiao et al., 2008a; Lin et al., 2012; Cao et al., 2016). Supporting this assessment, expression of the gain-of-function TRPV3 mutants in cells or pharmacologic activation of TRPV3 in cultured keratinocytes led to cell death (Xiao et al., 2008a; Cao et al., 2016; Szöllösi et al., 2018; Yan et al., 2019). Conversely, the characteristic epidermal hyperplasia found in OS patients (Lin et al., 2012) and hyperkeratosis seen in the TRPV3 gain-of-function mutant rodents (Asakawa et al., 2006) would argue for a proliferative function of this channel, a notion supported by a

¹Department of Critical Care Medicine, Shengjing Hospital of China Medical University, Shenyang, China; ²Department of Integrative Biology and Pharmacology, McGovern Medical School, The University of Texas Health Science Center at Houston, Houston, TX; ³School of Basic Medicine and Clinical Pharmacy, China Pharmaceutical University, Nanjing, China; ⁴State Key Laboratory for Chemistry and Molecular Engineering of Medicinal Resources, School of Chemistry and Pharmacy, Guangxi Normal University, Guilin, China.

Correspondence to Michael X. Zhu: michael.x.zhu@uth.tmc.edu; Bin Zang: zangbin66@aliyun.com; Jin-Bin Tian: jin.bin.tian@uth.tmc.edu.

© 2020 Wang et al. This article is distributed under the terms of an Attribution–Noncommercial–Share Alike–No Mirror Sites license for the first six months after the publication date (see <http://www.rupress.org/terms/>). After six months it is available under a Creative Commons License (Attribution–Noncommercial–Share Alike 4.0 International license, as described at <https://creativecommons.org/licenses/by-nc-sa/4.0/>).

recent study (Wang et al., 2020). This would be in line with the findings that TRPV3 exists in a protein complex with transforming growth factor- α and epidermal growth factor receptors in skin keratinocytes, and ablation of the *Trpv3* gene in mice leads to wavy hair coat and curly whiskers due to impaired hair follicle development and reduced epidermal permeability barrier because of the impaired keratinocyte cornification (Cheng et al., 2010).

Another common feature found in both OS patients and mutant rodents is enhanced cutaneous inflammation with infiltrating immune cells (Asakawa et al., 2006; Lin et al., 2012; Eytan et al., 2014; Wakabayashi et al., 2017). Whereas the proinflammatory cytokine release resulting from TRPV3 function (Xu et al., 2006; Szöllösi et al., 2018) may account for the enhanced immune cell infiltration and further increase in proinflammatory cytokines/chemokines, the inflammation might also affect TRPV3 channel function, as in the case of TRPV1. Since tissue acidosis is accompanied with inflammation and acid is well known to activate TRPV1, it is also pivotal to know how protons regulate TRPV3. Although TRPV3 was originally found not to be activated by extracellular protons (Smith et al., 2002), later studies demonstrated proton regulation of TRPV3 in multiple fashions (Cao et al., 2012; Gao et al., 2016). First, TRPV3 could be activated by glycolic acid, which penetrated the plasma membrane and then acted through intracellular acidification in a manner that partly involved an N-terminal histidine, H426 (Cao et al., 2012), a residue also known to be critical for TRPV3 activation by 2-aminoethoxydiphenyl borate (2-APB; Hu et al., 2004, 2009). Second, cytoplasmic residues L508, D512, S518, and A520, located within the S2–S3 linker, are important for weak activation of TRPV3 by intracellular protons in the absence of an agonist (Gao et al., 2016). Third, uniquely for 2-APB-based drugs, protons induce a configuration change of 2-APB that favors the drug binding to TRPV1, -V2, and -V3 channels, thereby strongly potentiating the agonist-evoked TRPV3 activation (Gao et al., 2016). Fourth, protons also inhibit TRPV3, which was seen at lower pH than that used to potentiate the channel activation and as the “off” response right after the wash-off of the acidic solution (Cao et al., 2012; Gao et al., 2016). However, critical residue(s) responsible for the proton inhibition of TRPV3 remains unknown.

To gain a more complete understanding of proton regulation of TRPV3 channels, we systematically scanned protonatable residues in the extracellular loops and several of them in the cytoplasmic C terminus of TRPV3 by substituting them with neutral amino acids. By performing whole-cell voltage-clamp recording of WT and mutant TRPV3 expressed in HEK293 cells stimulated with TRPV3 agonists, 2-APB (Hu et al., 2004), and carvacrol (Xu et al., 2006), we determined that D641, located at the selectivity filter of TRPV3, is critical for the extracellular proton inhibition of this channel, and that three negatively charged residues at the proximal C terminus of TRPV3, E682, E689, and D727 are important for switching the channel from the naive closed state to sensitized state based on their protonation status. These findings offer important insights into the molecular mechanism of TRPV3 regulation. Part of the findings has been reported in abstract form (Wang, H., Q. Wang, J. Tian, and M.X. Zhu. 2019. Mechanism of proton inhibition of TRPV3. *Abstr. 2653. Biophys. J.* 116:535a).

Materials and methods

Expression constructs and transfection in HEK293 cells

Full-length murine TRPV3 was isolated and subcloned into pIRES2-EGFP (Clontech) as previously described (Hu et al., 2004). TRPV3 mutations were made by using either a PCR-based approach or a QuikChange XL site-directed mutagenesis kit (Agilent Technologies). All mutations were verified by DNA sequencing.

HEK293 cells were grown in Dulbecco's modified Eagle's medium containing 4.5 mg/ml glucose, 10% heat-inactivated FBS, 50 U/ml penicillin, and 50 μ g/ml streptomycin. For electrophysiological experiments, cells were seeded in 35-mm culture dishes and transfected with the desired cDNA constructs using Lipofectamine 2000 (Invitrogen) following the protocol provided by the manufacturer or a polyethylenimine method as previously described (Feng et al., 2014). For intracellular Ca^{2+} measurements, cells were transfected with the desired cDNA constructs in the wells of 96-well plates without preseeding using Lipofectamine 2000 (Invitrogen) as described (Hu et al., 2004).

Intracellular Ca^{2+} measurements

Transiently transfected HEK293 cells in 96-well plates were washed once with an extracellular solution (ECS) containing 140 mM NaCl, 5 mM KCl, 1 mM MgCl_2 , 2 mM CaCl_2 , 10 mM glucose, and 10 mM HEPES, pH 7.4, and then incubated in 50 μ l ECS that was supplemented with 5 μ M Fluo-4/AM, 0.02% Pluronic F-127 (Molecular Probes), and 0.1% BSA at 37°C for 60 min. Probenecid (2 mM; Sigma-Aldrich) was included in all solutions to prevent dye leakage from the cells. At the end of the incubation, cells were washed three times with ECS and placed in 80 μ l of the same wash solution. Intracellular Ca^{2+} concentration changes were measured with a fluid-handling integrated fluorescence plate reader, FlexStation (Molecular Devices; Hu et al., 2004). The acidic compound solution contained 140 mM NaCl, 5 mM KCl, 1 mM MgCl_2 , 2 mM CaCl_2 , 10 mM glucose, and 30 mM Mes, pH 4.0. When 40 μ l of the acidic solution was delivered to the sample plate with 80 μ l ECS by the integrated robotic eight-channel pipettor, the final pH of the solution was 5.6 as determined by using a pH meter in parallel experiments after mixing ECS and the acidic solution at the same ratio.

2-APB (Cayman Chemical) or carvacrol (Sigma-Aldrich) was dissolved at 0.5 mM in DMSO and diluted in ECS or the acidic solution to three times the desired final concentrations and delivered at a half of the sample volume to the sample plate by the integrated robotic eight-channel pipettor at the pre-programmed time points. Multiple agonist concentrations were tested in parallel in different wells, with each well receiving the agonist only once. Fluo-4 fluorescence was read at an excitation of 494 nm and emission of 525 nm from the bottom of the plate at 0.67 Hz. Fluorescence increase in response to 2-APB (at both pH 7.4 and 5.6) or carvacrol (at pH 7.4) was quantified as the area under the curve and normalized to the maximal response from the same plate. Data from three independent experiments— independent transfections— were pooled to construct the agonist concentration–response curves. Half-maximal effective concentration (EC_{50}) values were derived by fitting the data points with the Hill equation.

Electrophysiologic recordings

Transfected HEK293 cells were reseeded on 12-mm round glass coverslips (Warner Instruments) 1 d after transfection. Whole-cell recordings were performed the following day. Recording pipettes were pulled from micropipette glass (Sutter Instruments) to 2–4 M Ω when filled with the internal solution containing (in mM) 140 CsCl, 1.0 MgCl₂, 1 EGTA, and 10 HEPES, pH 7.2, and placed in the bath solution composed of (in mM) 140 NaCl, 5 KCl, 2 CaCl₂, 1 MgCl₂, 10 glucose, and 10 HEPES, pH 7.4. Isolated cells were voltage clamped in the whole-cell mode by using an EPC9 (HEKA Instruments) amplifier. Voltage commands were made from the Patchmaster program (HEKA Instruments), and the currents were recorded at 5 or 10 kHz. For some recordings, voltage ramps of 200 ms to +100 mV after a brief (20 ms) step to –100 mV from holding potential of 0 mV were applied every second. For others, voltage ramps of 500 ms to +80 mV after a brief (100 ms) step to –80 mV from holding potential of 0 mV were applied every 2 s. Cells were continuously perfused with the bath solution during seal formation and break-in through a homemade gravity-driven perfusion system with the outlet placed ~50 μ m from the cell being recorded.

After establishing the whole-cell configuration, the external solution was switched to a nominally Ca²⁺-free solution containing (in mM) 140 NaCl, 5 KCl, 1 MgCl₂, 10 glucose, and 10 HEPES, pH 7.4, or a divalent cation-free (DVF) solution containing (in mM) 140 NaCl, 5 KCl, 10 glucose, and 10 HEPES, pH 7.4. The acidic solutions contained (in mM) 140 NaCl, 5 KCl, 1 MgCl₂, 10 glucose, and 10 HEPES (for pH 6.5 and pH 5.5) or 10 Mes (for pH 5.0), with pH adjusted to the desired values. For acidic DVF solutions, MgCl₂ was omitted. TRPV3 activator—2-APB or carvacrol—was diluted in the nominally Ca²⁺-free external solution, DVF solution, and the acidic solutions at the desired final concentrations and applied to the cell through perfusion. For recordings with intracellular pH (pH_i) clamped to 6.0 and 6.5, the pipette solutions were the same as the standard internal solution except that pH was adjusted to 6.0 and 6.5, respectively.

For recording from excised inside-out patches, a symmetrical Cs⁺-based solution containing (in mM) 140 CsCl, 1 MgCl₂, 1 EGTA, and 10 HEPES, pH 7.4, was used for both bath and pipette solutions. Patches were excised from HEK293 cells that expressed WT or mutant mouse TRPV3. Single-channel currents were recorded using a gap-free protocol at the desired holding voltage. Macroscopic currents were recorded from inside-out patches using voltage ramps of 200 ms to +100 mV after a brief (20 ms) step to –100 mV from holding potential of 0 mV, applied every second. Acidic solutions (in mM: 140 CsCl, 1 MgCl₂, 1 EGTA, and 10 HEPES, pH 5.5 or 6.5) were applied to the cytoplasmic side of the patch. The NMDG solution contained (in mM) 140 NMDG-Cl, 1 EGTA, and 10 HEPES, pH 7.4. All experiments were performed at room temperature (22–24°C).

Simulations

Unbiased (conventional MD simulations) and biased (metadynamics) simulations were performed as previously described (Wang et al., 2018). In brief, all systems were built by the System Builder module of DESMOND (Shaw, 2005). The structures

were embedded in a 1-palmitoyl-2-oleoyl-sn-glycero-3-phosphocholine lipid bilayer and then solvated into an orthorhombic box (13 Å in every dimension) filled with transferable intermolecular potential three-point water molecules. NaCl (150 mM) was added to the system to mimic physiologic conditions. All unbiased simulations were conducted under 300 K and 1 bar pressure using DESMOND (Shaw, 2005). The reversible reference system propagator algorithm integrator was used with a time step of 1 fs. The Berendsen algorithm was chosen for thermostat and barostat to maintain pressure at 1 bar. Non-bonded interactions were cut off at 12 Å. The trajectory recording interval was set to 200 ps and other default parameters were used during unbiased simulation runs.

The metadynamics analysis (Laio and Parrinello, 2002; Laio and Gervasio, 2008) was conducted by program DESMOND (Shaw, 2005) with a constant number of particles, pressure (1 bar) and temperature (300 K), and periodic boundary conditions by using Nose-Hoover chain Thermostat and Martyna-Tobias-Klein Barostat methods. The height and width of the Gaussian and the interval were set to 0.12 kcal/mol, 0.05 Å, and 0.09 ps, respectively. Before the simulation, the built systems were relaxed by using the default protocol of DESMOND in the following sequence: (1) NVT ensemble with Brownian dynamics for 100 ps at 10 K with small time step and solute heavy atom restrained; (2) NVT ensemble with a Berendsen thermostat for 12 ps at 10 K with small time step and solute heavy atom restrained; (3) NPT ensemble with a Berendsen thermostat and barostat for 12 ps at 10 K and 1 atm with solute heavy atom restrained; (4) NPT ensemble with a Berendsen thermostat for 12 ps at 300 K and 1 atm with solute heavy atom restrained; and (5) NPT ensemble with a Berendsen thermostat for 24 ps at 300 K and 1 atm with no restraints. After the relaxation, the metadynamic runs were protracted for ~60,000 ps until they showed free diffusivity along the defined collective variables (CVs), which indicates the convergence of metadynamic runs. This criterion was chosen according to the guidelines of assessing the accuracy of metadynamic runs (Laio et al., 2005).

All simulations were run on a DELL T7910 graphic workstation (with NVIDIA Tesla K40C-GPU). Preparation, analysis, and visualization were performed on a 12-CPU CORE DELL T7500 graphic workstation. The sum of the Gaussians and the free-energy surface were generated by the metadynamics analysis tools of DESMOND.

Data analysis

All summary data are presented as means \pm SEM, except when indicated otherwise, for *n* independent recordings. Statistical analyses were performed using Student's *t* test or one-way ANOVA with Bonferroni's multiple comparisons test. *P* < 0.05 is considered statistically significant. Graphs were generated by GraphPad Prism.

Results

Dual effect of extracellular acid on the activation of recombinant TRPV3

To examine the effect of protons on TRPV3, we first tested how application of an acidic solution affected 2-APB-evoked

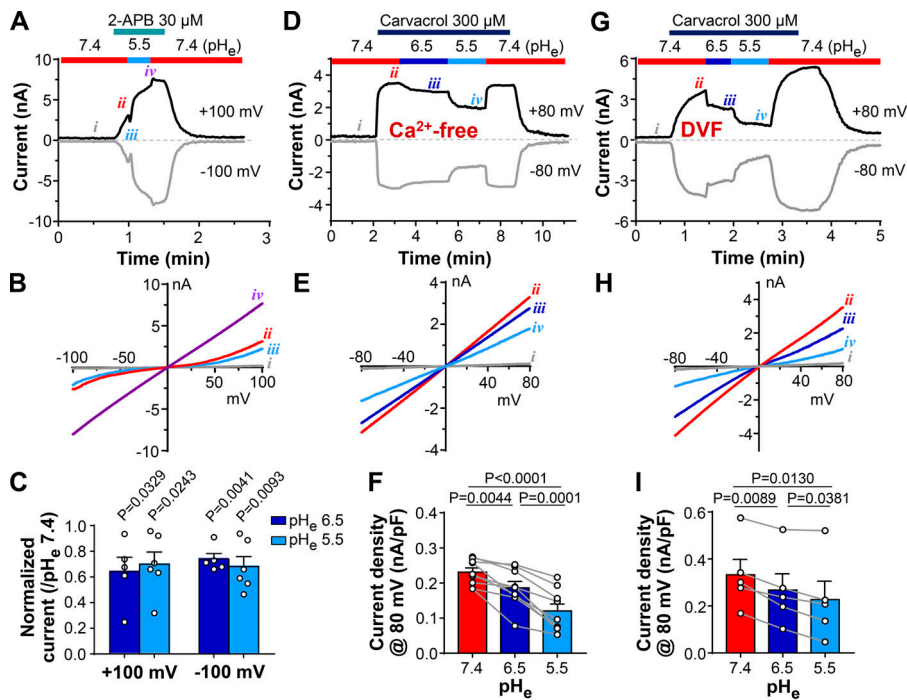


Figure 1. Proton inhibition of TRPV3. (A–F) HEK293 cells transiently expressing WT mouse TRPV3 were subject to whole-cell voltage-clamp recordings in nominally Ca²⁺-free bath solutions. Cells were exposed to 30 μM 2-APB (A and B) or 300 μM carvacrol (D–F) as indicated in the horizontal bars above the current traces shown in A and D. The pH of the external solution (pH_e) was 7.4 initially and then changed to 5.5 and 6.5 as indicated. A and D show representative traces of time courses of current amplitudes at +100 and –100 mV (A) and at +80 and –80 mV (D). B and E show I–V relationships at the indicated time points obtained by the voltage ramp. C is a summary of A for the initial decrease of 2-APB-evoked currents at +100 and –100 mV upon switching to pH_e 6.5 and pH_e 5.5 compared with that at pH_e 7.4 immediately before the pH change. Individual data points and means ± SEM are shown. P values were determined by using a one-sample *t* test with each sample group compared with the hypothetical value of 1. F is a summary of D for current density at steady state of carvacrol-evoked responses at +80 mV when pH_e was 7.4, 6.5, or 5.5. P values were determined by using a one-way ANOVA with Bonferroni’s multiple comparisons test. **(G–I)** Similar to D–F, but for carvacrol-evoked currents in a DVF bath solution. The same protocol was used as in D but Mg²⁺ was omitted from the nominally Ca²⁺-free bath solution.

whole-cell currents in HEK293 cells transiently expressing mouse TRPV3. To readily detect the agonist-evoked TRPV3 current, we omitted Ca²⁺ from the ECSs. As shown in Fig. 1 A, at the normal pH of 7.4, 30 μM 2-APB evoked slowly developing TRPV3 currents. The I–V curves showed double rectification and a reversal of around 0 mV (Fig. 1 B), typical for TRPV3-mediated nonselective currents (Xiao et al., 2008b). Upon application of a 5.5-pH solution with the same concentration of 2-APB, the currents first decreased and then rapidly increased to reach a quasi-steady state (Fig. 1 A), reflecting the dual effects of extracellular protons on 2-APB-evoked TRPV3 activation. The initial decrease reveals an inhibitory effect of protons, which is also evident from the “off” response upon removal of the 5.5-pH solution (Fig. 1 A), a phenomenon noted previously (Cao et al., 2012; Gao et al., 2016). The subsequent increase after the initial dip was due to proton modification of the 2-APB compound that favors the sp² coordination of the boron atom to confer a triangular planar configuration in acidic environment, rather than the tetrahedral shape coordinated by the sp³ geometry at the neutral pH (Gao et al., 2016). Despite the complex behaviors, proton inhibition was detected in all cells tested at both pH 5.5 and 6.5, and at both negative and positive potentials (Fig. 1 C). However, the concurrent potentiation did interfere with the accurate assessment of the degree of inhibition at the different pH or proton concentrations.

Since the proton potentiation was agonist specific (Gao et al., 2016), to avoid this effect, we used another TRPV3 agonist, carvacrol (Xu et al., 2006). Carvacrol is a weak agonist of TRPV3. Even at 300 μM and in the nominally Ca²⁺-free bath solution,

the first response of TRPV3-expressing cells to carvacrol was very small, which precludes an accurate assessment of the inhibitory action of protons. To overcome this problem, we took the advantage that TRPV3 currents are increased upon repeated stimulations (Xu et al., 2002; Xiao et al., 2008b) by treating the cells several times with 2-APB and carvacrol before the acid test. In these presensitized cells, carvacrol (300 μM) induced robust TRPV3 currents (Fig. 1 D), with the linear I–V relationship indicating the full sensitization of the channel (Fig. 1 E). This allowed for more accurate evaluation of the inhibition without the confounding effect of continued sensitization. Under these conditions, sequential application of 6.5- and 5.5-pH solutions resulted in the dose-dependent suppression of carvacrol-evoked TRPV3 currents, with pH 5.5 causing ~50% decrease at +80 mV compared with pH 7.4 (Fig. 1, D and F). Previously, Mg²⁺ was shown to suppress TRPV3 currents from both extracellular and intracellular sides (Luo et al., 2012). To examine if Mg²⁺ included in the Ca²⁺-free bath solution impacts the proton inhibition of TRPV3, we also used a DVF bath solution. As shown in Fig. 1, G–I, protons still inhibited carvacrol-evoked TRPV3 currents in the DVF solution.

Asp641 mediates extracellular proton inhibition of TRPV3

Typically, protons regulate protein functions by altering conformations through protonation at glutamate (E), aspartate (D), or histidine (H) residues. To determine which of the protonatable residues is involved in the proton regulation of TRPV3 function, we neutralized all extracellular glutamates, aspartates, and histidines of TRPV3 (Fig. 2, A and B) by mutagenesis and

then tested low pH-induced changes in 2-APB-induced responses for all mutant channels transiently expressed in HEK293 cells by using a cell-based high-throughput Ca^{2+} assay performed on microplates (Miller et al., 2011; Gao et al., 2016). Based on the concentration–response curves for 2-APB in 7.4- and 5.6-pH solutions, we determined EC_{50} values and found that all extracellular mutations tested maintain the sensitivity to protonated 2-APB, showing enhancement in the apparent affinity (Fig. 2 D). Among them, the E610Q and E631A mutants displayed decreased sensitivity to 2-APB compared with WT TRPV3 at both pH 7.4 and pH 5.6. We also tested TRPV3 F654A, because its equivalent F659 in rat TRPV1—F660 for human and mouse TRPV1—is critical for voltage-dependent activation and potentiation by protons (Aneiros et al., 2011). However, TRPV3 F654A also exhibited reduced sensitivity to 2-APB without affecting proton potentiation, and the E610Q/F654A double mutant worked similarly as individual E610Q and F654A single mutants (Fig. 2 D). Thus, although some of the tested residues may be important for channel gating by 2-APB or other stimuli, the extracellular protonatable residues of TRPV3 do not contribute to proton potentiation. This is consistent with the previous finding that the proton potentiation of 2-APB activation of TRPVs occurs at the ligand level rather than receptor level (Gao et al., 2016).

Among the mutants, D641N exhibited the greatest difference (~21-fold) between EC_{50} values obtained in the acidic and neutral solutions, higher than that of the WT channel (~15-fold; Fig. 2 D). Given that D641 is located in the selectivity filter of the TRPV3 channel and has been shown to be important for regulation by extracellular cations, such as Ca^{2+} , Mg^{2+} , and ruthenium red (Chung et al., 2005; Xiao et al., 2008b; Luo et al., 2012), we reasoned that it might also mediate proton regulation such that the enhanced proton potentiation could imply a loss of proton inhibition. To corroborate this idea, we measured the effects of extracellular acidification on whole-cell currents of TRPV3 D641N elicited by either 2-APB (30 μM) or carvacrol (300 μM). As shown in Fig. 3, A–C, even at pH 5.0, the acidic solution no longer caused the initial dip of 2-APB-evoked current in D641N, as seen in the WT channel. For the carvacrol-evoked D641N current, application of acidic solutions of pH 6.5 and pH 5.5 during the drug treatment also failed to reduce the current amplitude in both the nominally Ca^{2+} -free and DVF bath solutions (Fig. 3, D–F). These data suggest that D641 is the critical residue involved in the extracellular proton inhibition of TRPV3.

Neutralization of cytoplasmic C-terminal protonatable residues enhances TRPV3 activity

We have previously shown that under conditions used for experiments in Fig. 2 D, pH_i also decreases due to both extracellular acidification and the treatment of 2-APB, although the effect of 2-APB is much weaker than that of extracellular protons (Gao et al., 2016). Given that protons were reported to activate TRPV3 from the cytoplasmic side and amino acid residues at the N terminus and S2–S3 linker have been implicated in this effect (Cao et al., 2012; Gao et al., 2016), we asked if the protonatable residues at the C terminus also play a role. Therefore, we neutralized selected C-terminal glutamates and aspartates

immediately downstream from the S6 helix (Fig. 2, A and C). Interestingly, two single mutants, E689Q and D727N, showed reduced EC_{50} for 2-APB at both pH 7.4 and pH 5.6 in the Ca^{2+} assay (Fig. 2 D), and this effect was maintained with a combination of E689Q and D727N, or E682Q with either E689Q or D727N or E689Q and D727N together, although E682Q itself did not show enhancement in the apparent affinity to 2-APB (Fig. 2 D). Surprisingly, these double and triple mutants showed greatly reduced ratios (<4.6) for EC_{50} values obtained at pH 7.4 and pH 5.6 compared with the WT channel (~15), and for the triple mutant (E682Q/E689Q/D727N, hereafter referred to as QQN), the ratio was even close to 1 (0.92; Fig. 2 D), suggesting that the proton potentiation might be lost.

In whole-cell voltage-clamp recordings, we detected increased currents in cells that expressed E682Q, E689Q, or D727N, or their double or triple combinations, in response to 30 μM 2-APB at pH 7.4 compared with those that expressed WT TRPV3 (Fig. 4). Proton potentiation (by pH 6.5) was detected in all constructs except for the E689Q/D727N double mutant, and for the QQN triple mutant, potentiation was very weak (Fig. 4, G–I). Proton inhibition was observed at the beginning of the acidic solution application in all cells, but the degree and duration of the inhibition were variable such that in some cells (e.g., Fig. 4 G) the dip could barely be seen.

Both the diminished proton inhibition and proton potentiation in the E689Q/D727N double and QQN triple mutants were unexpected if the inhibition is mediated by D641, as demonstrated above (Fig. 3), and the potentiation is due to proton modification of the 2-APB ligand, instead of the channel, according to previous findings (Gao et al., 2016). The limited degree of intracellular acidification caused by lowering extracellular pH to 6.5 in whole-cell conditions was unlikely to markedly affect protonatable residues at the cytoplasmic side of the channel; therefore, there must be other reasons for the apparent loss of proton inhibition and potentiation seen in the Ca^{2+} assay and whole-cell recordings for these mutants. We reasoned that the variability might reflect the issue that the 1-s intervals used to construct the time course from currents that were recorded using voltage ramps were too infrequent to capture the fast changes in proton inhibition and potentiation at this 2-APB concentration; therefore, we tested QQN with 5 μM 2-APB. At this low 2-APB concentration, both the inhibition and potentiation by acid were slowed down. At pH 7.4, 2-APB slowly elicited currents in cells that expressed QQN and the switch to pH 6.5 strongly suppressed the current first and then slowly enhanced it (Fig. 5 A). Although cells expressing WT TRPV3 also exhibited similar response patterns, the current amplitudes were markedly smaller than that in QQN-expressing cells (Fig. 5 E). If the QQN-expressing cells were exposed to the 6.5-pH bath solution before the application of 2-APB, an obvious delay was observed before the current development (Fig. 5 B). Quantification of the slope of current increase indicated that the currents at both negative and positive potentials developed significantly faster in 6.5-pH solution than in 7.4-pH solution (Fig. 5 C); however, the delay time between 2-APB application and the current development was also significantly longer in the 6.5-pH solution (Fig. 5 D).

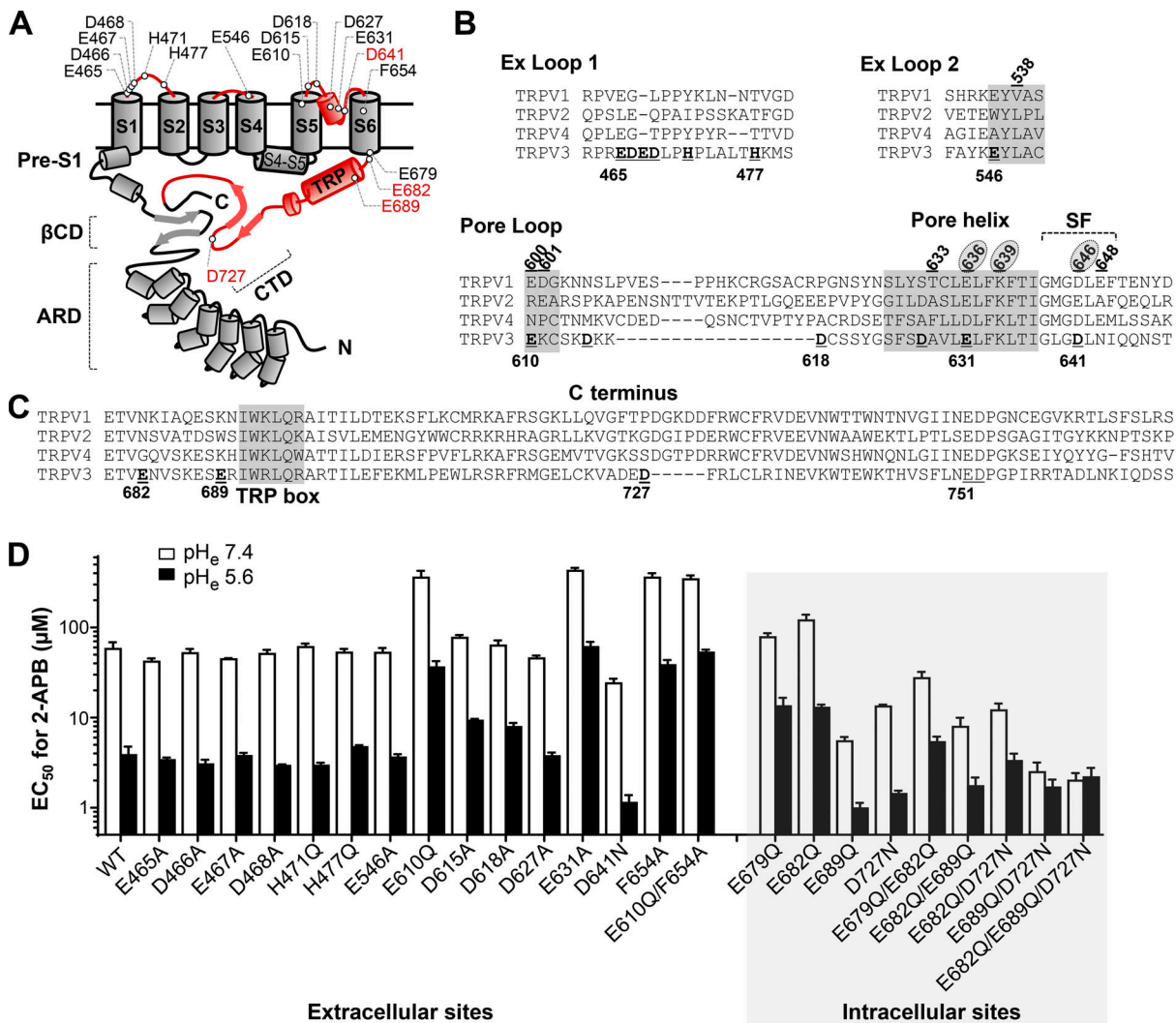


Figure 2. Mutational analysis of protonatable sites of TRPV3. (A) Diagram of the TRPV3 protein depicting transmembrane segments S1–S6 and amino acid residues in the extracellular loops and C terminus mutated in the current study. Cylinders and arrows indicate α helices and β strands, respectively, incorporating information from the recent cryo-EM structures of apo TRPV3 (PDB accession no. 6MHO and 6DVW). Amino acid sequences in the red portions are shown in B and C. Key functional amino acids for proton regulation found in the current study are highlighted in red. While D641 mediates extracellular proton inhibition, the neutralization of E682, E689, and D727 stabilizes the channel in a sensitized state. Note the intra-molecular interaction between CTD and β CD. (B) Amino acid alignment of mouse TRPV1–V4 at extracellular (Ex) loops 1 and 2 and the pore loop. Mutated residues of TRPV3 in the current study are underlined. Residues implicated in proton regulation of TRPV1 are marked on top of the sequences with the amino acid numbers (numbering according to rat TRPV1) indicated and those involved in inhibition highlighted with gray ovals. Shaded sequence areas are contained within α -helices based on the recent cryo-EM structures (PDB accession no. 6MHO and 6DVW). Locations of pore helix and selectivity filter (SF) are also indicated. (C) Amino acid alignment of mouse TRPV1–V4 at the C-terminal portion that encompasses E679 to S769 of TRPV3. E682, E689, and D727 of TRPV3 are underlined. E751 and D752, which form interprotomer salt bridge with K169 to stabilize the apo state, are also underlined. The conserved TRP box, which is contained within the TRP helix is shaded. (D) EC₅₀ values of 2-APB obtained from cell-based Ca²⁺ assay performed at 7.4 pH of the external solution (pH_e; open bars) and 5.6 pH_e (filled bars) on HEK293 cells that transiently expressed WT mouse TRPV3 and its mutants as indicated. The assays were performed in 96-well microtiter plates. Results from two independent transfections, each performed in triplicate, were pooled after normalization to the maximal response. EC₅₀ values were derived from fitting the means of the normalized responses at different 2-APB concentrations with the Hill equation. Error bars represent SE of the fits, representing the precision of the fitted values. The shaded area at right shows results of C-terminal mutations. ARD, ankyrin repeat domain; S4–S5, S4–S5 linker; TRP, TRP helix.

The above data indicate that the C-terminal mutations did not eliminate the proton inhibition and potentiation of 2-APB-induced TRPV3 response, except for the increase in apparent affinity that makes 30 μ M 2-APB nearly saturating. This would be consistent with the Ca²⁺ assay showing that the E689Q/D727N and QQN mutants had lower EC₅₀ values than the WT channel (Fig. 2 D). However, the similar EC₅₀ values for 2-APB at neutral and acidic pH observed for these mutants is in

conflict with the notion that acid potentiates 2-APB-evoked activation of TRPV1, -V2, and -V3 through modification of the configuration of the 2-APB compound (Gao et al., 2016) and the finding from whole-cell recordings using 5 μ M 2-APB (Fig. 5, A–C). To find the reason for this discrepancy, we inspected the time courses of fluorescence changes at pH 7.4 and pH 5.6 for cells stimulated with submaximal 2-APB concentrations, which should best reveal any potentiation effect. At pH 7.4, the Ca²⁺

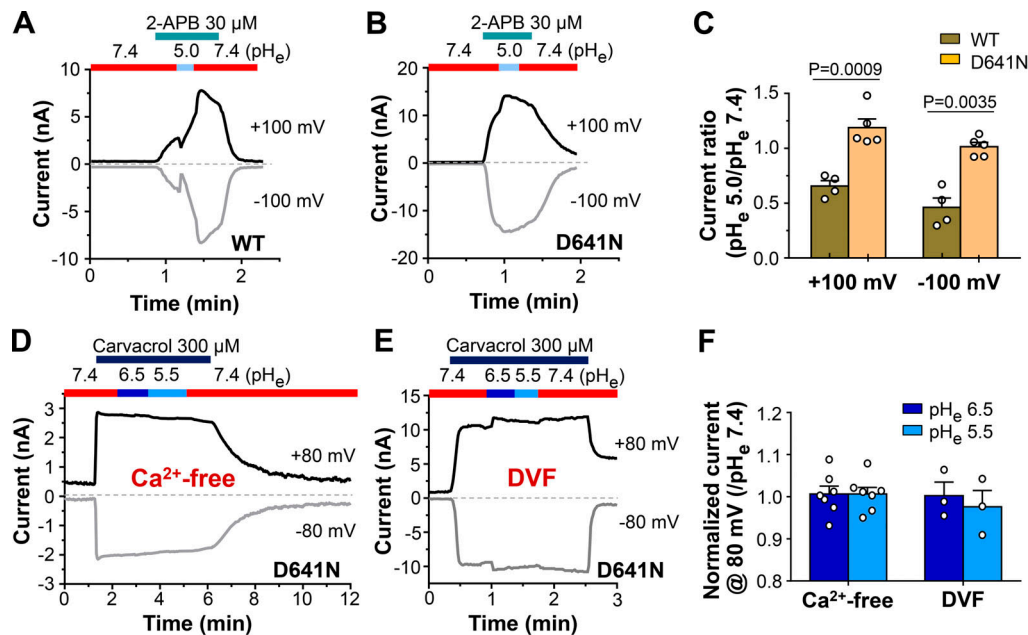


Figure 3. Asp641 mediates proton inhibition of TRPV3. (A–F) HEK293 cells transiently expressing WT or D641N of mouse TRPV3 were subject to whole-cell voltage-clamp recordings in nominally Ca²⁺-free (A, B, and D) or DVF (E) bath solutions. Cells were exposed to 30 μM 2-APB (A–C) or 300 μM carvacrol (D–F) as indicated in the horizontal bars above the current traces shown in A, B, D, and E. The pH of the external solution (pH_e) was initially 7.4 and then changed to 5.0, 5.5, and 6.5 as indicated. A, B, D, and E show representative traces of time courses of current amplitudes at +100 and –100 mV (A and B) and at +80 and –80 mV (D and E). C shows a summary of A and B for the immediate (the first second) change of 2-APB-evoked currents at +100 and –100 mV upon switching to 5.0 pH_e for cells that expressed WT and D641N TRPV3. Individual data points and means ± SEM for ratio of currents at pH_e 5.0/7.4 are shown. P values were determined by unpaired t test. F shows a summary of D and E for steady-state carvacrol-evoked currents at +80 mV in pH_e 6.5 and 5.5, normalized to that at pH_e 7.4, for cells that expressed D641N and were recorded in the nominal Ca²⁺-free (left) and DVF (right) solutions.

responses to 3 and 10 μM 2-APB of cells that expressed E689Q/D727N and QQN were comparable to that of cells expressing the WT channel stimulated with 30 and 100 μM 2-APB, respectively (Fig. 5 F), which is in line with the increased affinity of the mutant channels. Lowering extracellular pH to 5.6 markedly increased the fluorescence intensity in all the cells, which is indicative of acid potentiation, but in the E689Q/D727N- and QQN-expressing cells, the increase was transient, declining to the initial level in ~1 min for the 10 μM 2-APB-stimulated cells (Fig. 5 F, right two panels). By contrast, cells expressing WT TRPV3 and E682Q/D727N exhibited relatively sustained Ca²⁺ responses at pH 5.6 (Fig. 5 F, left two panels). Also notable is that the E689Q/D727N and QQN mutants exhibited slow desensitization even at pH 7.4, which was not seen in the WT channel (Fig. 5 F). Since the EC₅₀ values shown in Fig. 2 D were based on dose–response relationships constructed using the area under the curve from the Ca²⁺ assay, the rapid desensitization in the acidic solution of the E689Q/D727N and QQN mutants would yield lower measures of the total area and thus a lower estimate of the proton potentiation effect. This explains the apparent lack of acid potentiation in the Ca²⁺ assay for these mutants.

In the Ca²⁺ assay, carvacrol did not induce a fluorescence increase in WT-TRPV3-expressing cells until the concentration was increased to ≥100 μM (Fig. 6, A and B); however, in cells that expressed E682Q/D727N, E689Q/D727N, or QQN mutants, Ca²⁺ responses were elicited by lower carvacrol concentrations. For E682Q/727N, E689Q/D727N, and QQN, we determined EC₅₀ values to be 196.7 ± 7.8 μM (n = 4), 60.2 ± 3.2 μM (n = 4), and 118.8

± 7.6 μM (n = 6), respectively (Fig. 6, A and B). For WT TRPV3, EC₅₀ could not be reliably determined because of the limited number of data points with detectable activities. Thus, combining the Ca²⁺ assay data for both 2-APB and carvacrol, as well as the electrophysiological data for 2-APB at 5 and 30 μM, it is clear that charge neutralization of E682, E689, and D727 at the C terminus of TRPV3 enhanced the sensitivity of the channel to both of its agonists, 2-APB and carvacrol. As with the stimulation by 2-APB (Fig. 5 A), the amplitude of carvacrol-evoked current in cells that expressed QQN was consistently decreased by extracellular acidification (Fig. 6, C and D), again indicating that the C-terminal mutations do not abolish inhibition by protons.

It was previously shown that protons also directly activate TRPV3 from the cytoplasmic side through residues at the S2–S3 linker (Gao et al., 2016). To test if the C-terminal mutations affected direct proton activation, we performed inside-out recording using patches excised from cells that expressed WT TRPV3 and the E689Q/D727N or QQN mutant. In patches from WT-expressing cells, we detected sparse single-channel currents in symmetric Cs⁺-based, Ca²⁺-free solutions that contained 1 mM MgCl₂ with pH set at 7.4 (Fig. 7 A). The single-channel currents exhibited a linear I–V relationship with a slope conductance of 168.2 ± 3.9 pS (Fig. 7 C), similar to that reported for TRPV3 (158 pS and 165 pS) in Mg²⁺-free solutions (Cao et al., 2012; Luo et al., 2012). Lowering pH at the cytoplasmic side to 6.5 and 5.5 dramatically increased the open probability of the WT TRPV3 channel by several fold (Fig. 7, A and B), consistent with the previous observation (Gao et al., 2016). Although there was a

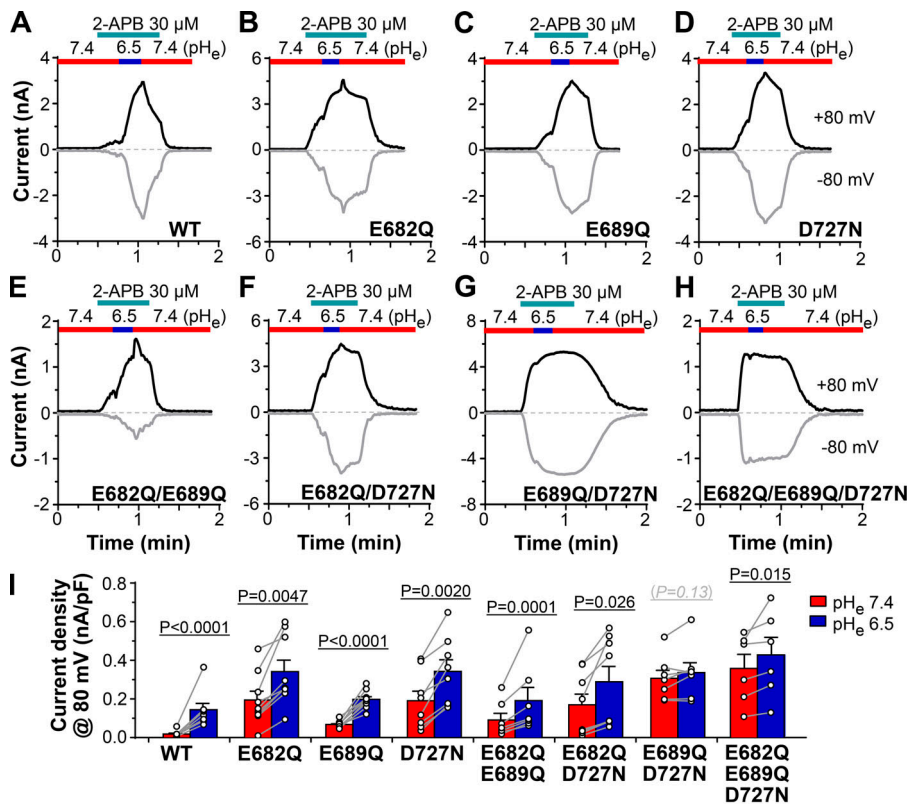


Figure 4. C-terminal mutations enhance 2-APB-evoked TRPV3 current. HEK293 cells transiently expressing WT TRPV3 or its C-terminal mutants as indicated were subject to whole-cell voltage-clamp recordings in nominally Ca²⁺-free bath solutions. Cells were exposed to 30 μM 2-APB as indicated in the horizontal bars above the current traces. The pH of the external solution (pH_e) was initially 7.4 and then changed to 6.5 as indicated. **(A–H)** Representative traces of time courses of current amplitudes at +80 and –80 mV. **(I)** Summary of current density at +80 mV in pH_e 7.4 immediately before switching to pH_e 6.5 and at the end of the pH_e 6.5 exposure for WT TRPV3 and its C-terminal mutants. Individual data points and means ± SEM are shown. P values were determined by ratio paired t test for each construct. Only E689Q/D727N had P > 0.05 (highlighted in parenthesis).

weak trend for the unitary current to decrease in the acidic solutions, the changes were not statistically significant (Fig. 7D).

On the other hand, in patches excised from cells that expressed E689Q/D727N or QQN, we consistently recorded macroscopic currents, of which the outward current was largely abolished by switching the bath (cytoplasmic) solution to one that contained NMDG⁺ as the only cation, indicative of cation selectivity (Fig. 7, E and F). Thus, in excised patches, the mutant channels showed strong constitutive activity, a phenomenon not observed in whole-cell recordings. More importantly, and in contrast to the WT channel, the constitutive currents of the E689Q/D727N and QQN mutants were strongly inhibited by the 5.5-pH solution applied to the cytoplasmic side, although the effect of the 6.5-pH solution was not obvious. These data suggest that the mutant channels are prone to spontaneous activation in the inside-out configuration and such high basal activity occludes proton activation of TRPV3 from the cytoplasmic side.

Protonation of E682, E689, and D727 facilitates sensitization of TRPV3

The increased sensitivity to agonists and strong constitutive activity in inside-out patches suggest that neutralization of the three acidic C-terminal residues likely has an impact on TRPV3 channel conformation so that it is easier to open than when the three residues are negatively charged. It should be mentioned that the currents shown in Figs. 4, 5, and 6 represent the responses of individual cells that had been exposed to 2-APB for the first time. This suggests that the C-terminal mutations might exist in a somewhat sensitized state instead of the naive state as

often seen for the WT TRPV3 channel. To test this possibility, we compared the responses of WT TRPV3 and the QQN mutant to repeated exposures to carvacrol. As shown in Fig. 8, A and B, whereas the WT channel took ~14 repeated stimulations to approach the maximal response to 300 μM carvacrol, QQN reached the highest level of response even with the first stimulation by this drug, which supports the idea that neutralization of the three acidic residues converts the channel from a naive non-sensitized state to a sensitized one.

Since protonation neutralizes the negative charges of acidic residues, we predicted that by protonating the acidic residues, intracellular acidification should also sensitize the TRPV3 channel. To test this hypothesis, we used pipette solutions with pH adjusted to either 6.5 or 6.0 and performed repeated stimulations of the WT channel again using carvacrol. As shown in Fig. 8 C, with pH_i set at 6.0, it only took five repeated stimulations for the WT channel to approach the maximal response to 300 μM carvacrol. At pH_i 6.5, the sensitization was also accelerated compared with the normal pH_i of 7.2, but the effect was more modest (Fig. 8 D). Therefore, protonation from the intracellular side accelerates TRPV3 sensitization to repeated agonist stimulation.

Recently, several high-resolution structures of human and mouse TRPV3 have been made available by using single-particle cryo-EM (Zubcevic et al., 2018, 2019; Singh et al., 2018, 2019). These structures include ligand-free closed (or apo) state, putative sensitized states by either 2-APB or heat, and open states by introducing a point mutation Y564A (Singh et al., 2018, 2019), revealing great details of TRPV3 channel conformational changes that may be associated with the transition from naive to

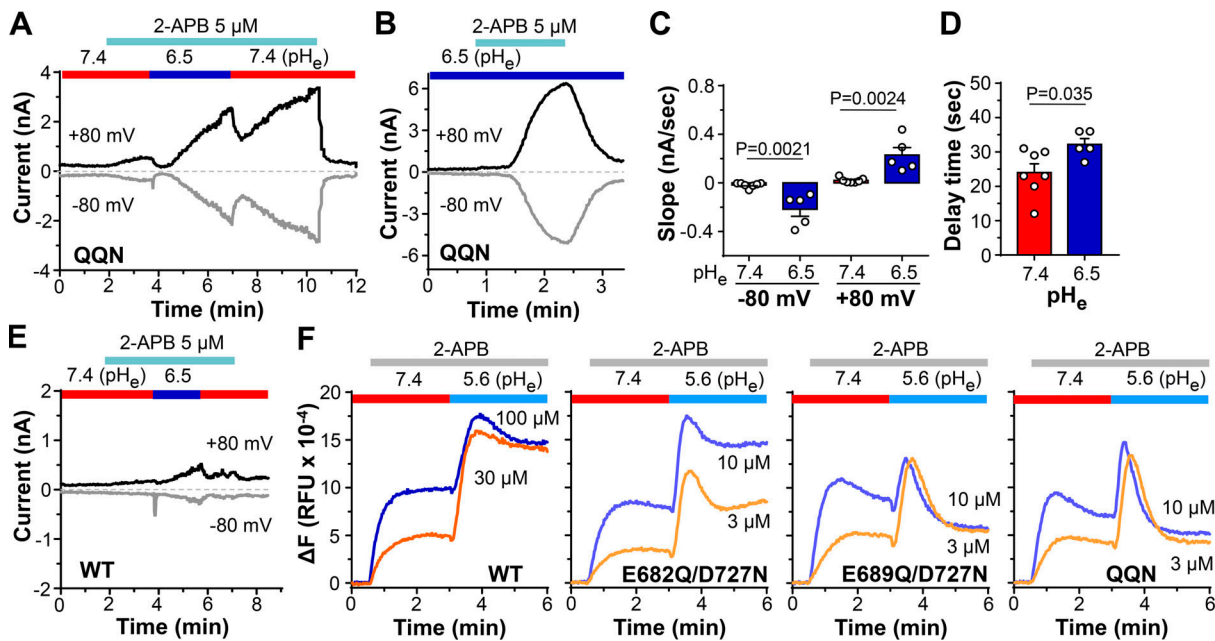


Figure 5. C-terminal mutations do not abolish proton inhibition and potentiation to 2-APB-evoked TRPV3 response. (A–D) HEK293 cells transiently expressing the E682Q/E689Q/D727N (QQN) mutant of TRPV3 were subject to whole-cell voltage-clamp recordings in nominally Ca²⁺-free bath solutions. The pH of the external solution (pH_e) was either 7.4 (A) or 6.5 (B) when 5 μM 2-APB was applied as indicated. In A, pH_e was also changed to 6.5 and then back to 7.4 during the continued presence of 2-APB as indicated. Of note, there was slow inhibition and then potentiation of the currents at pH_e 6.5. In B, note the ~30-s delay in current development after the addition of 2-APB. C shows a summary of A and B for slope during the rising phase of current development at –80 mV and +80 mV at pH_e 7.4 and 6.5. Individual data points and means ± SEM are shown. P values were determined by unpaired *t* test. D shows a summary of A and B for time lapse between the beginning of 2-APB addition and the time point when *di/dt* started to exceed 2 over the next 10 data points for current measured at +80 mV. Individual data points and means ± SEM are shown. P value was determined by unpaired *t* test. **(E)** Similar to A, but for a cell that expressed WT TRPV3. **(F)** Representative traces of Ca²⁺ response in cells that expressed WT TRPV3 or its C-terminal mutants as indicated. Cells were bathed in ECS containing 2 mM Ca²⁺, pH 7.4, when 2-APB was added, then acidic solution with the same concentration of 2-APB was added to make the final pH_e to 5.6. 2-APB concentrations are indicated next to the traces. Note the fast desensitization of E689Q/D727N and QQN, especially in the low pH condition.

sensitized, and from closed to open states. However, because the functionality of the particles in cryo-EM images is typically untested, some structures that were considered to represent sensitized states could rather be inactivated states. Interestingly, E682 is located at the C-terminal end of the S6 transmembrane helix only five residues downstream from the narrowest part of the channel pore formed by M677 in the closed state, which constitutes the lower gate (Zubcevic et al., 2018; Singh et al., 2018). In the apo state, an interhelical loop (or turn) exists around E682 to allow the connected TRP helix to be parallel to the plasma membrane (Fig. 9, A–D), but in the sensitized and open states, E682 is incorporated into the extended α-helical turn from the S6 helix, which either continues into the TRP helix (Zubcevic et al., 2018, 2019) or is briefly disrupted right before the TRP helix (Singh et al., 2018, 2019). As a result, E689, which is right before the conserved TRP box (marked in Fig. 2 C) found in most TRP proteins, either resides within the TRP helix (Zubcevic et al., 2018, 2019) or becomes a part of a loop preceding the TRP helix, especially in the open state (Singh et al., 2018, 2019). Of note, the location of the lower gate and whether it is the main activation gate of TRPV3 (Jara-Oseguera et al., 2019) have been challenged by the latest TRPV3 structures determined in lipid nanodisc showing that I674 in S6 constitutes the lower gate and G638 in the selectivity filter forms the upper gate (Deng et al., 2020; Shimada et al., 2020).

Further inspection of these structures also revealed that, in the structure of 2-APB-bound mouse TRPV3 (Protein Data Bank [PDB] accession no. 6DVY, which represents either sensitized/closed or an inactivated state), salt-bridge interactions and/or hydrogen bonds (H-bond) exist between the side chains of E682 and K686 and between the side chains of E689 and R693 and those of E689 and Q570. These bonds may be disrupted in the 2-APB-bound open state (PDB accession no. 6DVZ; Singh et al., 2018). D727, in contrast, is located at the open part of a hairpin that dives into the cavity created between the ankyrin repeat domain and coupling domain β-sheet (βCD; see Fig. 2 A) at the N terminus. It has been shown that this region undergoes a large conformational change between the apo and sensitized states (Zubcevic et al., 2019), and the changes in the interaction between the N- and C-terminal sequences here have been found to affect the heat response of TRPV3 (Macikova et al., 2019). In the apo structure of mouse TRPV3, the side chain of C721 forms an H-bond with the carboxyl group in the side chain of D727 (PDB accession no. 6DVW), which is switched to the backbone carbonyl of D727 in the 2-APB-bound closed state (PDB accession no. 6DVY) and then to the backbone carbonyl of E726 in the 2-APB-bound open state (PDB accession no. 6DVZ; Singh et al., 2018). Therefore, all three residues—E682, E689, and D727—appear to localize in areas of the TRPV3 channel that undergo large conformational changes between naive and sensitized or

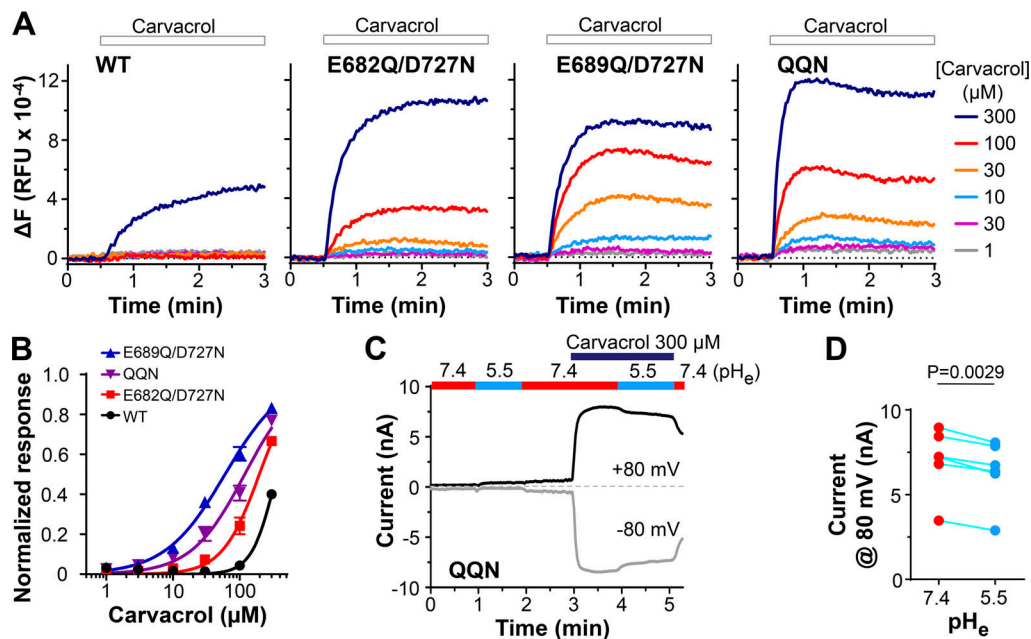


Figure 6. C-terminal mutations enhance carvacrol-evoked TRPV3 response. (A) Representative traces of Ca^{2+} response in cells that expressed WT TRPV3 or its C-terminal mutants as indicated. Cells were bathed in ECS containing 2 mM Ca^{2+} , pH 7.4, when carvacrol was added at different concentrations as indicated to the right of the rightmost graph. Note that for cells expressing WT TRPV3, the response was only observed at the highest concentration of carvacrol used (300 μM). (B) Concentration–response curves constructed based on the Ca^{2+} assay shown in A. Data points represent means \pm SEM of $n = 6$ for WT and QQN, and $n = 4$ for E682Q/D727N and E689Q/D727N, respectively. Solid lines represent fits by the Hill equation. (C) Acid inhibition of carvacrol-evoked QQN current. HEK293 cells transiently expressing TRPV3 QQN mutant were subject to whole-cell voltage-clamp recordings in nominally Ca^{2+} -free bath solutions with the pH of the external solution (pH_e) 7.4 and 5.5 as indicated in the horizontal bars above the current trace. Carvacrol (300 μM) was applied as indicated. (D) Summary of current amplitudes in the presence of carvacrol in pH 7.4 (red) immediately before switching to pH_e 5.5 and at the end of the pH_e 5.5 application (blue). P value was determined by ratio paired t test.

open states, and protonation will likely impact the free energy distributions in these states due to changes in H-bonds. However, since the side chains and H-bonds in the cryo-EM structures are incompletely resolved, the aforementioned structural changes should be taken with caution.

To assess how neutralization of E682, E689, and D727 affects the C-terminal structure and free energy distribution of TRPV3, we performed MD and metadynamic simulations on WT TRPV3 and the QQN mutant based on the structure templates of apo (resting) and sensitized human TRPV3 (Zubcevic et al., 2018), which provide better resolution and more complete side chain information in the C-terminal regions than other TRPV3 structures found in the PDB. The metadynamic simulations allow for studying the mechanism of chemical reactions and the best pathway of protein conformational transitions by reconstructing 3-D maps based on free energy changes during these processes (Laio and Parrinello, 2002). Between the resting and sensitized human TRPV3 (Zubcevic et al., 2018), the $C_\alpha - C_\alpha$ distances of E682_{chains_A,C} and E682_{chains_B,D} undergo marked changes from 17.6 Å to 14.5 Å (Fig. 9, A–C), reflective of a loop-to-helical transition in this area (Fig. 9 D). In metadynamic stimulations of free energy changes of $C_\alpha - C_\alpha$ distances of E682_{chains_A,C} (CV1) and E682_{chains_B,D} (CV2) modeled after the sensitized human TRPV3 structure, we found the lowest free energy states to deviate markedly from the initial 14.5 Å in WT TRPV3, but for QQN, the 14.5-Å distances represented the lowest energy (Fig. 9, E and F). This suggests that the QQN mutant is

more stable in the sensitized state than the WT TRPV3. In addition, with unbiased conventional MD simulations (~ 450 ns) performed in the WT and mutant channels, and protein secondary structure elements, like α -helices and β -strands, monitored throughout simulations, we detected that the likelihood of α -helix formation around E682 to E689 is higher in QQN than in the WT TRPV3 (Fig. 9, G and H). Thus, the observations in both the biased (metadynamic) and unbiased simulations are consistent with the idea that the QQN mutant adapts a sensitized state, characterized by the closer distance among E682 C_α 's and the extension of the S6 helix to the TRP helix that encompasses the E682 to E689 region, as suggested by the cryo-EM structures (Zubcevic et al., 2018, 2019; Singh et al., 2018).

Discussion

Protons affect conformation of all proteins, but only those that have functional impact are of biological significance. While the effects of protons on TRPV3 function have been illustrated previously (Cao et al., 2012; Gao et al., 2016), these effects are complex and molecular mechanisms remain elusive. For the closely related TRPV1, proton sensing is one of the major properties associated with the physiologic function of this channel (Tominaga et al., 1998). Although critical amino acids involved in the acid-evoked TRPV1 activation found in extracellular loops of the TRPV1 protein include both protonatable and non-protonatable ones (Fig. 2 B; Jordt et al., 2000; Ryu et al., 2007),

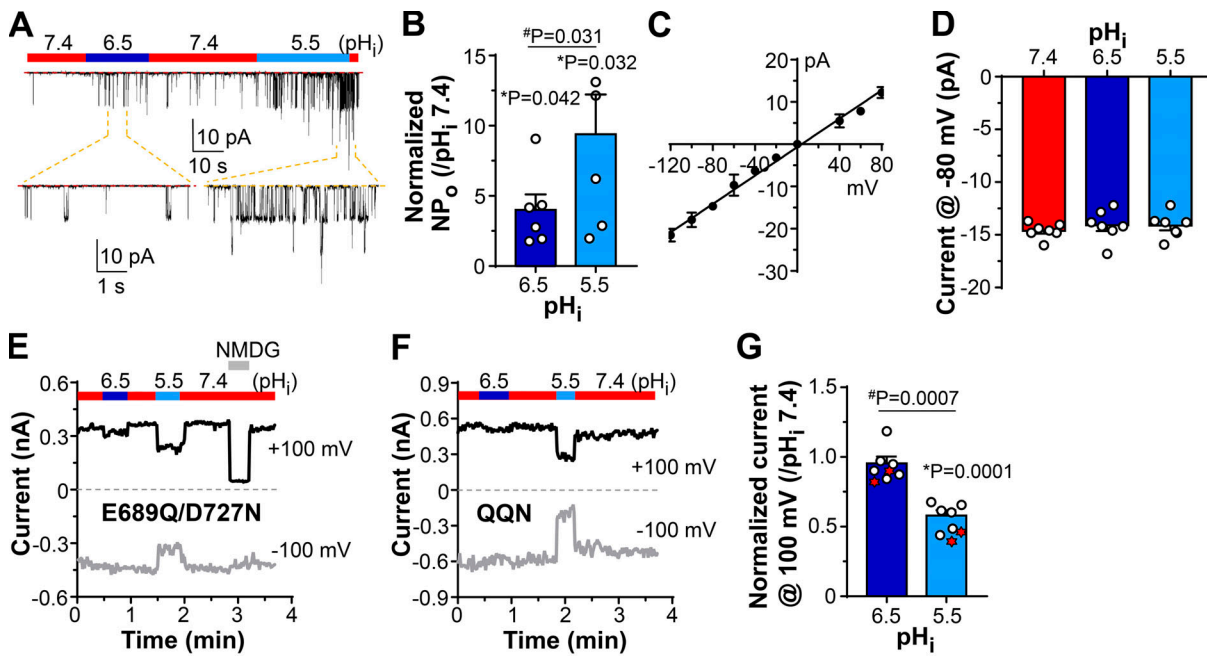


Figure 7. C-terminal mutations enhance constitutive activity of TRPV3 in inside-out patches. (A) Representative traces of single-channel currents recorded at the holding potential of -80 mV from inside-out patches excised from HEK293 cells that expressed WT TRPV3. pH_i was initially set at 7.4 and then changed to 6.5 and 5.5 as indicated. Lower traces show sections indicated by the dashed lines in an expanded time scale. (B) Summary of fold changes in NP_o at pH_i 6.5 and 5.5 compared with that at pH_i 7.4. Individual data points and means \pm SEM are shown. *, P values determined by one-sample *t* test with the sample group compared with the hypothetical value of 1; #, P value for pH_i 5.5 versus pH_i 6.5 by paired *t* test. NP_o , open probability of the channel where N represents the number of channels. (C) Single-channel I-V relationship of WT TRPV3 measured from inside-out patches at pH_i 7.4. Data points represent means \pm SD of three to five patches. Solid line is the fit by linear regression. (D) Single-channel amplitudes at -80 mV for conditions shown in A. Individual data points and means \pm SEM are shown. (E and F) Macroscopic currents recorded from inside-out patches excised from HEK293 cells that expressed E689Q/D727N (E) and QQN (F) mutants of TRPV3. Currents were elicited by voltage ramps as that used for whole-cell recording. No agonist was applied, but pH_i was changed from 7.4 to 6.5 and then 5.5 as indicated. NMDG⁺ was added as indicated to replace the conducting cation (Cs⁺) at the cytoplasmic side. (G) Summary of E and F for ratios of current amplitudes at $+100$ mV of pH_i 6.5/ pH_i 7.4 and pH_i 5.5/ pH_i 7.4. Individual data points (white circles) and means \pm SEM are shown for E689Q/D727N. *, P value determined by one-sample *t* test with the sample group compared with the hypothetical value of 1; #, P value for pH_i 5.5 versus pH_i 6.5 by paired *t* test. Individual data points for QQN (red stars) are overlaid but not included in the statistical analysis.

testing the protonatable residues represents the common and effective initial strategy to explore the potential mechanism of proton regulation (Jordt et al., 2000; Liu et al., 2009). By mutating the negatively charged residues, Asp, Glu, and His, to

Asn, Gln, or Ala, the substitution neutralizes the charge at the neutral pH, thereby mimicking the effect of protonation of the original residues at the acidic pH. This provided the rationale for experiments conducted in the current study.

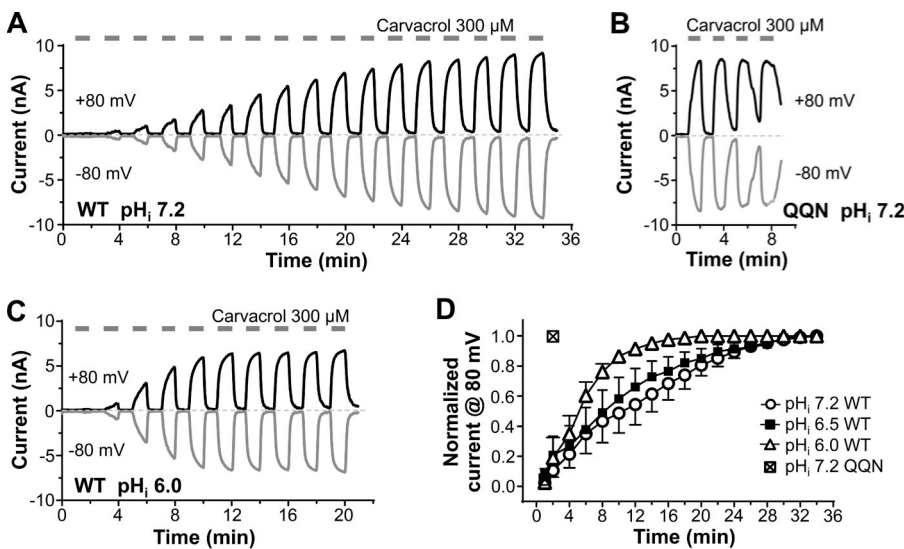


Figure 8. Intracellular acidification facilitates sensitization of TRPV3. HEK293 cells transiently expressing WT TRPV3 or its QQN mutant were subject to whole-cell voltage-clamp recordings in the external pH 7.4 nominally Ca²⁺-free bath solution, with pH_i set to 7.2, 6.5, or 6.0, as indicated, by the pipette solutions. The cell was repeatedly exposed to 30-s applications of 300 μ M carvacrol multiple times. (A–C) Representative traces of time courses of current amplitudes at $+80$ and -80 mV for WT (A and C) and QQN (B) at pH_i 7.2 (A and B) and pH_i 6.0 (C). (D) Summary of carvacrol-elicited peak current amplitudes at $+80$ mV normalized to the maximal response over time. Data are means \pm SEM for $n = 6$ cells. Errors are smaller than the symbols for some data points.

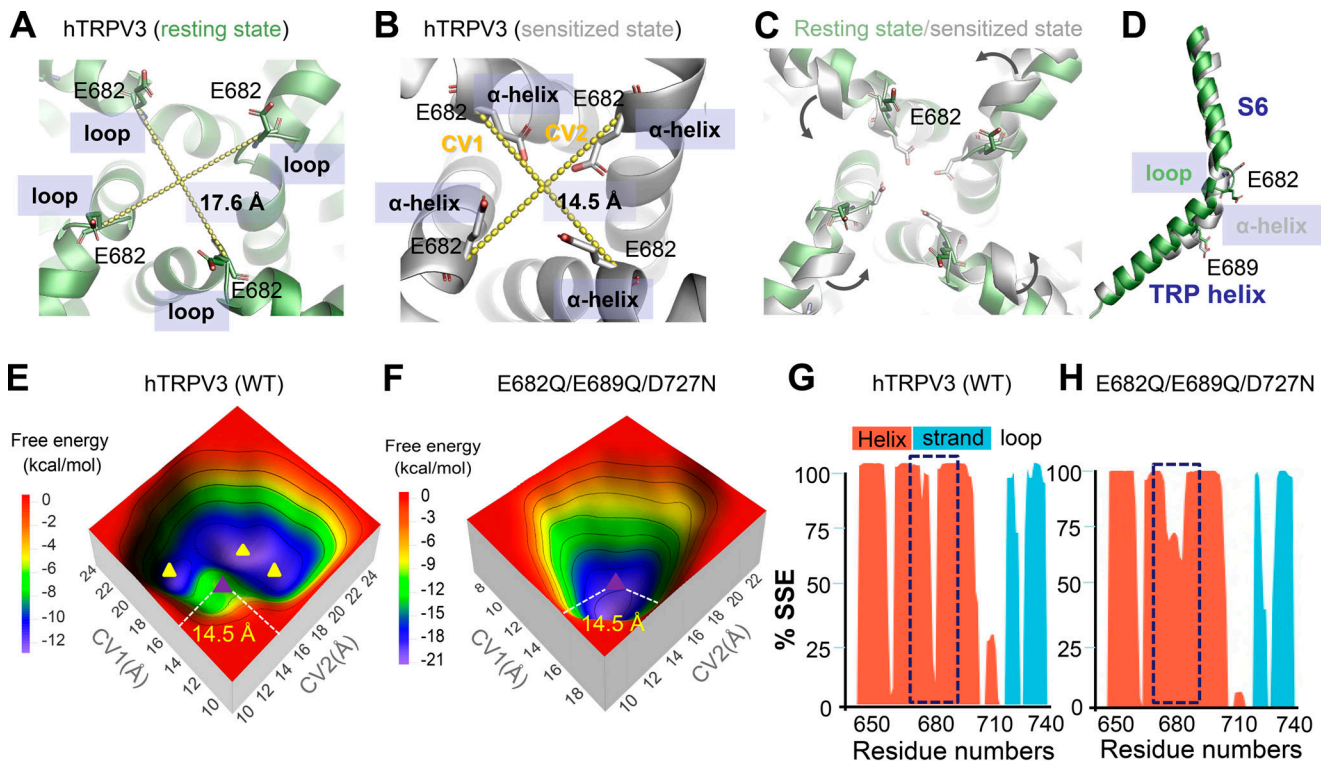


Figure 9. Metadynamic and conventional molecular dynamic (CMD) simulations of TRPV3 C-terminal structures. Computer simulations were performed based on the structures of apo (resting) and sensitized human TRPV3 (hTRPV3; PDB accession nos. 6MHO and 6MHS, respectively; Zubcevic et al., 2018). **(A and B)** $C_{\alpha} - C_{\alpha}$ distances of E682_{chain-A,C} (CV1) and E682_{chain-B,D} (CV2) of hTRPV3 in resting (A) and sensitized (B) states. **(C)** Overlay of resting (green) and sensitized (gray) states in the same regions covered in A and B, showing the rotation of S6 helix and E682. **(D)** A different view of S6 and TRP helices of a single protomer with resting (green) and sensitized (gray) states overlaid to show the loop-to- α -helix transition around E682. **(E and F)** Free energy landscape generated by metadynamic simulations of CV1 and CV2 of WT TRPV3 (E) and the QQN mutant (F) modeled after the sensitized hTRPV3 (PDB accession no. 6MHS). Note the presence of multiple low free-energy states (yellow triangles) in WT TRPV3, which are outside the initial state revealed by the cryo-EM structure. In QQN, however, the lowest free-energy state overlaps with the initial state (purple triangle). **(G and H)** CMD simulations of C-terminal regions of WT TRPV3 (G) and QQN mutant (H) for protein secondary structure elements (SSEs). The simulations initiated from the sensitized hTRPV3 structure and lasted for 450 ns. The likelihood of α -helix, β -strand, and loop are indicated by orange, cyan, and white, respectively. The area with large differences is highlighted in the rectangular boxes.

Our first main finding is that proton inhibition of TRPV3 is mediated by the aspartic residue, D641, located at the selectivity filter. We initially focused on the potentiation of 2-APB-evoked TRPV3 activity by extracellular acidification; however, by testing individual neutralization mutations of all protonatable residues located in the extracellular loops of mouse TRPV3 by using a cell-based Ca^{2+} assay, we did not find any mutation that exhibited a loss of the proton potentiation (Fig. 2 D). This finding is in line with the notion that the proton potentiation is ligand specific and the functionally critical modification occurs at the ligand (2-APB), instead of the receptor—that is, TRPV3 (Gao et al., 2016). However, we noticed that a previously studied mutant, D641N (Chung et al., 2005; Xiao et al., 2008b; Luo et al., 2012), not only displayed increased sensitivity (decreased EC_{50}) to 2-APB at the neutral pH compared with the WT channel, but an even greater decrease in the EC_{50} value at the acidic pH than at neutral (Fig. 2 D). With whole-cell recording, we confirmed that TRPV3 D641N exhibits a loss of proton inhibition whether it is activated by 2-APB or carvacrol and whether or not Mg^{2+} is present (Fig. 3), demonstrating that D641 is the critical site of TRPV3 inhibition by extracellular protons and that this inhibition is independent of Mg^{2+} (Fig. 1, G–I).

Interestingly, the equivalent residue of rat TRPV1, D646, has also been reported to be one of the key residues that mediate proton inhibition of the unitary conductance of TRPV1 channels (Liu et al., 2009), although the D647N mutation in mouse TRPV1—equivalent to D646 of rat TRPV1—only reduced but not completely eliminated proton inhibition (Lee and Zheng, 2015). Both TRPV3 D641 and TRPV1 D646 are located in the selectivity filter of the channel and are implicated in the regulation by polyvalent cations, such as Ca^{2+} and ruthenium red, among others, from the extracellular side (García-Martínez et al., 2000; Xiao et al., 2008b; Winter et al., 2013). In TRPV1, the proton inhibition involves two additional residues, E636 and K639, in the pore helix. The pore helices and the connected selectivity filters of TRPV1 and TRPV3 are quite conserved and, thus, the equivalent residues, E631 and K634, respectively, also exist in TRPV3 (Fig. 2 B). It is possible that these residues also contribute to proton inhibition of TRPV3. We have tested the effect of 5.0-pH solution on 2-APB-evoked activation of TRPV3 E631A. Indeed, the 5.0:7.4 pH ratio became 0.98 ± 0.09 at +100 mV and 1.02 ± 0.03 at -100 mV ($n = 3$), indicating a dramatically decreased proton inhibition by the neutralizing mutation. Because

of the reduced ligand sensitivity and small current density of E631A, we did not examine the proton effect on carvacrol-evoked activation of this mutant; however, based on the study of TRPV1 (Liu et al., 2009), it is likely that TRPV3 also uses the same conserved mechanism to suppress channel conductance in response to extracellular acidosis.

The reported reductions in single-channel conductance by protons applied to both inside-out and outside-out patches of TRPV3 (Cao et al., 2012), as in the case of TRPV1 (Liu et al., 2009), would be in agreement with the above assessment. However, under our experimental conditions with Cs⁺-based solutions that contained 1 mM Mg²⁺ and 1 mM EGTA, lowering pH at the cytoplasmic side did not significantly decrease the single-channel current amplitude at -80 mV (Fig. 7 D). Differences in the main charge carriers (Cs⁺ versus Na⁺), the presence and absence of EGTA and Mg²⁺, and holding potentials used (-80 versus +80 mV) might account for the different results between our study and the previous one (Cao et al., 2012). Nonetheless, in the sensitized human TRPV3 cryo-EM structures, the carboxyl group in the sidechain of E631 forms an H-bond with the backbone amide of D641 (see PDB accession nos. 6MHS [Zubcevic et al., 2018] and 6OT2 [Zubcevic et al., 2019]). Thus, disrupting this interaction by protonation or neutralization of E631 may alter the structural coordinates of D641 during gating. This implies that the E631A mutant might exert its effect on proton inhibition through structural changes at D641.

The near complete loss of proton potentiation in the Ca²⁺ assay for the E689Q/D727N and QQN mutants (Fig. 2 D) was a surprise, given the earlier finding that proton potentiation occurs at the level of boron-containing 2-APB compounds, rather than the TRPV3 channel (Gao et al., 2016). In whole-cell recordings, the proton potentiation effect was also barely observed at 30 μM (Fig. 4, G-I) but became evident at 5 μM 2-APB (Fig. 5, A-C), which is indicative of a saturation effect at 30 μM 2-APB, consistent with the decreased EC₅₀ values found in the Ca²⁺ assay for these mutants. That the E689Q/D727N and QQN mutants still possess proton potentiation is also evident from the time courses of Ca²⁺ responses showing the immediate rise of the fluorescence intensity upon lowering the extracellular pH in the presence of 2-APB; however, these two mutants also exhibited obvious desensitization, which was more pronounced in the acidic solution (Fig. 5 F). Furthermore, the activation of QQN currents by the low concentration of 2-APB was delayed in the acidic compared with the neutral solution (Fig. 5 D). Thus, in the mutant channels, proton inhibition manifests in several different forms—delayed activation, transient current suppression, and accelerated desensitization—to counter its potentiation effect on 2-APB-evoked activation. In quantifications based on the area under the curve, these inhibitory effects in combination yielded lower estimates of the drug potency and the apparent lack of proton-induced decreases in the EC₅₀ values.

The second main finding of the current study is that protonation of certain C-terminal residues facilitates sensitization of TRPV3. Our data suggest that neutralization of E682, E689, and D727 converts TRPV3 from the apo (or naive) state to a sensitized conformation. Not only did the QQN mutant exhibit enhanced sensitivity to agonists, but it also became robustly

activated upon first stimulation, in contrast to the WT channel that requires repeated stimulations to be sensitized (Fig. 8, A and B). In addition, both the E689Q/D727N and QQN mutants exhibited strong constitutive activity only in excised inside-out patches, suggesting that a diffusible factor may exist in the whole cell to keep the sensitized channels closed.

Sensitization to repetitive stimulation is a well-known feature of TRPV3 (Xu et al., 2002; Xiao et al., 2008b; Liu et al., 2011; Zubcevic et al., 2019). The naive and sensitized states of TRPV3 have been proposed to represent two distinguished closed conformations, C₀ and C₁, respectively, wherein the sensitization by repetitive stimulation may be explained by a gradual irreversible transition from the C₀ state to the C₁ state (Liu et al., 2011; Zubcevic et al., 2019). Recent studies have shown that sensitization of TRPV3 involves changing the conformation of the cytoplasmic domains to alter the interaction at the intersubunit interface (Macikova et al., 2019; Zubcevic et al., 2019). In particular, the interprotomer salt bridge between K169 in the ankyrin repeat domain and E751 and D752 in the distal portion of the C-terminal domain (CTD) is disrupted as part of a large rearrangement of CTD (Zubcevic et al., 2019). As illustrated in Fig. 2 A, CTD is downstream from the TRP helix and D727 is located in its proximal portion, at the opposite end of E751/D752 in the clamp that holds the N-terminal βCD in place in the apo state (Zubcevic et al., 2018, 2019). It is plausible that disrupting either end of the clamp will similarly weaken the molecular interactions between CTD and the βCD, which also weakens the aforementioned interprotomer salt bridge.

In addition, the transition from apo to sensitized state also involves a twist and rotation of the lower half of S6 helix, which may be accompanied with an α-to-π helical transition beginning at F666 in the middle of this helix (Zubcevic et al., 2018, 2019); however, in TRPV3 structures resolved in lipid nanodisc, the π-helix was also found in the apo state and only reverted to α-helix in an inactivated state (Deng et al., 2020; Shimada et al., 2020). As a result of the rotation of the S6 helix, E682, which is present in the interhelical loop between S6 and TRP helices in the apo state, is now incorporated into the S6 and continued through TRP helix (Zubcevic et al., 2018, 2019; also see Fig. 9 D). Also interesting is that the pre-TRP box α helical turn that contains E689 in the closed states becomes relaxed in the open state (Singh et al., 2018, 2019). These together with the changes in the structure and position of the hairpin that harbors D727, as well as the switches in the H-bonds associated with the carboxyl sidechains of the three acidic residues (Zubcevic et al., 2018, 2019; Singh et al., 2018, 2019), all suggest that these residues constitute a part of the conformational transition of the TRPV3 channel from the naive resting state to sensitization and/or open. Our simulation data indicate that neutralization of these residues not only stabilizes the reduced distances between E682 in different protomers that represent sensitized conformation, but also increases the loop-to-helix transition of the area from E682 to E689 (Fig. 9).

Since the charge neutralization mutations mimic protonation, we used acidic internal solutions to show that intracellular acidification indeed facilitates the sensitization process of WT TRPV3 (Fig. 8, C and D). This finding reveals a new aspect of

proton regulation of TRPV3 wherein protonation of C-terminal residues stabilizes the channel in the sensitized conformation, which leads to a greater response to the subsequent stimulation. Importantly, this mechanism of TRPV3 sensitization, which involves protonation of the cytoplasmic residues E682, E689, and D727 is distinct from the previously studied acid potentiation of 2-APB-evoked TRPV1, -V2, and -V3 channel activation, which arises through structural modification of the 2-APB-based ligand, rather than the channels (Gao et al., 2016).

Acidosis contributes not only to pain and inflammation, but to many other pathologic conditions as well (Holzer, 2009; Waldmann and Lazdunski, 1998; Wang and Xu, 2011). In particular, as cells that highly express TRPV3, skin keratinocytes are exposed to an acidic pH of around 5.5 (ranging from 4 to 7 pH) under physiologic conditions (Fiers, 1996). The acidity of human skin stratum corneum can reach pH 4.5 and it increases to normal pH at the first viable epidermal layer (stratum granulosum; Dikstein and Zlotogorski, 1994; Ohman and Vahlquist, 1994). Acidic microdomains are present in the extracellular matrix of the stratum corneum in the form of aqueous acidic pockets (Hanson et al., 2002). This acid mantle has been suggested to serve critical functions for the permeability barrier homeostasis and normal integrity of the skin, in addition to being antimicrobial (Hachem et al., 2003; Fluhr et al., 2004). Given the demonstrated role of TRPV3 in keratinocyte cornification and skin barrier formation (Cheng et al., 2010), it is remarkable that TRPV3 channel function displays a strong sensitivity to environmental pH changes. Moreover, decreases in pH_i have long been known to accompany hypoxia, inflammation, and neurodegeneration (Taggart and Wray, 1998; Fang et al., 2010). Therefore, a thorough understanding of pH regulation of the TRPV3 channel is very important.

The current study provides novel mechanistic insights into how protons exert an inhibitory effect through D641 at the selectivity filter and how three acidic residues at the proximal C terminus, E682, E689, and D727, affect channel conformation through protonation such that the charge neutralization shifts the channel from the naive resting state to a sensitized one primed for more robust activation. The complex responses to acidification may be critical for regulating TRPV3 channel function at the appropriate levels, as both the loss and the gain of function of TRPV3 have been shown to cause morphologic alteration and impair skin function.

Acknowledgments

Joseph A. Mindell served as editor.

We are grateful to our colleagues for comments and discussions. We thank Dr. Guangwei Du (University of Texas Health Science Center at Houston, Houston, TX) for providing the polyethylenimine reagent.

This work was supported in part by grants from the National Institutes of Health (DK081654, NS092377, and NS102452 to M.X. Zhu) and Guangxi Funds for Distinguished Experts (to Y. Yu).

The authors declare no competing financial interests.

Author contributions: conceptualization: J.-B. Tian., Y. Yu, and M.X. Zhu; data curation: H. Wang, P. Yang, Y. Lu, J. Wang,

J. Jeon J.-B. Tian, Y. Yu, and M.X. Zhu; formal analysis: H. Wang, P. Yang, Y. Lu, J. Wang, J. Jeon, Q. Wang, J.-B. Tian, Y. Yu, and M.X. Zhu; funding acquisition: Y. Yu and M.X. Zhu; investigation: H. Wang, P. Yang, Y. Lu, J. Wang, J.-B. Tian, B. Zang, Y. Yu, and M.X. Zhu; project administration: Y. Yu and M.X. Zhu; supervision: J.-B. Tian, B. Zang, Y. Yu, and M.X. Zhu; validation: H. Wang, P. Yang, Y. Lu, J.-B. Tian, and Y. Yu; visualization: H. Wang, P. Yang, Y. Lu, J. Wang, J.-B. Tian, B. Zang, Y. Yu, and M.X. Zhu; writing, original draft: M.X. Zhu; writing, review and editing: all authors.

Submitted: 18 May 2020

Revised: 7 October 2020

Accepted: 17 November 2020

References

- Aneiros, E., L. Cao, M. Papakosta, E.B. Stevens, S. Phillips, and C. Grimm. 2011. The biophysical and molecular basis of TRPV1 proton gating. *EMBO J.* 30:994–1002. <https://doi.org/10.1038/emboj.2011.19>
- Asakawa, M., T. Yoshioka, T. Matsutani, I. Hikita, M. Suzuki, I. Oshima, K. Tsukahara, A. Arimura, T. Horikawa, T. Hirasawa, and T. Sakata. 2006. Association of a mutation in TRPV3 with defective hair growth in rodents. *J. Invest. Dermatol.* 126:2664–2672. <https://doi.org/10.1038/sj.jid.5700468>
- Bandell, M., L.J. Macpherson, and A. Patapoutian. 2007. From chills to chilis: mechanisms for thermosensation and chemesthesis via thermoTRPs. *Curr. Opin. Neurobiol.* 17:490–497. <https://doi.org/10.1016/j.conb.2007.07.014>
- Cao, X., F. Yang, J. Zheng, and K. Wang. 2012. Intracellular proton-mediated activation of TRPV3 channels accounts for the exfoliation effect of α -hydroxyl acids on keratinocytes. *J. Biol. Chem.* 287:25905–25916. <https://doi.org/10.1074/jbc.M112.364869>
- Cao, X., H. Wang, Y. Li, M. Lee, L. Jiang, Y. Zhou, C. Feng, Z. Lin, and Y. Yang. 2016. Semidominant Inheritance in Olmsted Syndrome. *J. Invest. Dermatol.* 136:1722–1725. <https://doi.org/10.1016/j.jid.2016.04.024>
- Caterina, M.J., M.A. Schumacher, M. Tominaga, T.A. Rosen, J.D. Levine, and D. Julius. 1997. The capsaicin receptor: a heat-activated ion channel in the pain pathway. *Nature.* 389:816–824. <https://doi.org/10.1038/39807>
- Cheng, X., J. Jin, L. Hu, D. Shen, X.P. Dong, M.A. Samie, J. Knoff, B. Eisinger, M.L. Liu, S.M. Huang, et al. 2010. TRP channel regulates EGFR signaling in hair morphogenesis and skin barrier formation. *Cell.* 141:331–343. <https://doi.org/10.1016/j.cell.2010.03.013>
- Chung, M.K., A.D. Güler, and M.J. Caterina. 2005. Biphasic currents evoked by chemical or thermal activation of the heat-gated ion channel, TRPV3. *J. Biol. Chem.* 280:15928–15941. <https://doi.org/10.1074/jbc.M500596200>
- Deng, Z., G. Makshev, M. Rau, Z. Xie, H. Hu, J.A.J. Fitzpatrick, and P. Yuan. 2020. Gating of human TRPV3 in a lipid bilayer. *Nat. Struct. Mol. Biol.* 27:635–644. <https://doi.org/10.1038/s41594-020-0428-2>
- Dikstein, S., and A. Zlotogorski. 1994. Measurement of skin pH. *Acta Derm. Venereol. Suppl. (Stockh.)*. 185:18–20.
- Eytan, O., D. Fuchs-Telem, B. Mevorach, M. Indelman, R. Bergman, O. Sarig, I. Goldberg, N. Adir, and E. Sprecher. 2014. Olmsted syndrome caused by a homozygous recessive mutation in TRPV3. *J. Invest. Dermatol.* 134:1752–1754. <https://doi.org/10.1038/jid.2014.37>
- Fang, B., D. Wang, M. Huang, G. Yu, and H. Li. 2010. Hypothesis on the relationship between the change in intracellular pH and incidence of sporadic Alzheimer's disease or vascular dementia. *Int. J. Neurosci.* 120:591–595. <https://doi.org/10.3109/00207454.2010.505353>
- Feng, X., Y. Huang, Y. Lu, J. Xiong, C.O. Wong, P. Yang, J. Xia, D. Chen, G. Du, K. Venkatachalam, et al. 2014. *Drosophila* TRPML forms PI(3,5)P₂-activated cation channels in both endolysosomes and plasma membrane. *J. Biol. Chem.* 289:4262–4272. <https://doi.org/10.1074/jbc.M113.506501>
- Fiers, S.A. 1996. Breaking the cycle: the etiology of incontinence dermatitis and evaluating and using skin care products. *Ostomy Wound Manage.* 42:32–34. 36:38–40 passim.
- Fluhr, J.W., M. Mao-Qiang, B.E. Brown, J.P. Hachem, D.G. Moskowitz, M. Demerjian, M. Haftek, G. Serre, D. Crumrine, T.M. Mauro, et al. 2004. Functional consequences of a neutral pH in neonatal rat stratum

- corneum. *J. Invest. Dermatol.* 123:140–151. <https://doi.org/10.1111/j.0022-202X.2004.22726.x>
- Gao, L., P. Yang, P. Qin, Y. Lu, X. Li, Q. Tian, Y. Li, C. Xie, J.B. Tian, C. Zhang, et al. 2016. Selective potentiation of 2-APB-induced activation of TRPV1-3 channels by acid. *Sci. Rep.* 6:20791. <https://doi.org/10.1038/srep20791>
- García-Martínez, C., C. Morenilla-Palao, R. Planells-Cases, J.M. Merino, and A. Ferrer-Montiel. 2000. Identification of an aspartic residue in the P-loop of the vanilloid receptor that modulates pore properties. *J. Biol. Chem.* 275:32552–32558. <https://doi.org/10.1074/jbc.M002391200>
- Hachem, J.P., D. Crumrine, J. Fluhr, B.E. Brown, K.R. Feingold, and P.M. Elias. 2003. pH directly regulates epidermal permeability barrier homeostasis, and stratum corneum integrity/cohesion. *J. Invest. Dermatol.* 121:345–353. <https://doi.org/10.1046/j.1523-1747.2003.12365.x>
- Hanson, K.M., M.J. Behne, N.P. Barry, T.M. Mauro, E. Gratton, and R.M. Clegg. 2002. Two-photon fluorescence lifetime imaging of the skin stratum corneum pH gradient. *Biophys. J.* 83:1682–1690. [https://doi.org/10.1016/S0006-3495\(02\)73936-2](https://doi.org/10.1016/S0006-3495(02)73936-2)
- Holzer, P. 2009. Acid-sensitive ion channels and receptors. *Handb. Exp. Pharmacol.* 194:283–332. https://doi.org/10.1007/978-3-540-79090-7_9
- Hu, H.Z., Q. Gu, C. Wang, C.K. Colton, J. Tang, M. Kinoshita-Kawada, L.Y. Lee, J.D. Wood, and M.X. Zhu. 2004. 2-aminoethoxydiphenyl borate is a common activator of TRPV1, TRPV2, and TRPV3. *J. Biol. Chem.* 279:35741–35748. <https://doi.org/10.1074/jbc.M404164200>
- Hu, H., J. Grandl, M. Bandell, M. Petrus, and A. Patapoutian. 2009. Two amino acid residues determine 2-APB sensitivity of the ion channels TRPV3 and TRPV4. *Proc. Natl. Acad. Sci. USA.* 106:1626–1631. <https://doi.org/10.1073/pnas.0812209106>
- Jara-Oseguera, A., S.A. Simon, and T. Rosenbaum. 2008. TRPV1: on the road to pain relief. *Curr. Mol. Pharmacol.* 1:255–269. <https://doi.org/10.2174/1874467210801030255>
- Jara-Oseguera, A., K.E. Huffer, and K.J. Swartz. 2019. The ion selectivity filter is not an activation gate in TRPV1-3 channels. *eLife.* 8:e51212. <https://doi.org/10.7554/eLife.51212>
- Jordt, S.E., M. Tominaga, and D. Julius. 2000. Acid potentiation of the capsaicin receptor determined by a key extracellular site. *Proc. Natl. Acad. Sci. USA.* 97:8134–8139. <https://doi.org/10.1073/pnas.100129497>
- Laio, A., and F.L. Gervasio. 2008. Metadynamics: a method to simulate rare events and reconstruct the free energy in biophysics, chemistry and material science. *Rep. Prog. Phys.* 71:126601. <https://doi.org/10.1088/0034-4885/71/12/126601>
- Laio, A., and M. Parrinello. 2002. Escaping free-energy minima. *Proc. Natl. Acad. Sci. USA.* 99:12562–12566. <https://doi.org/10.1073/pnas.202427399>
- Laio, A., A. Rodriguez-Fortea, F.L. Gervasio, M. Ceccarelli, and M. Parrinello. 2005. Assessing the accuracy of metadynamics. *J. Phys. Chem. B.* 109:6714–6721. <https://doi.org/10.1021/jp045424k>
- Latorre, R., S. Brauchi, G. Orta, C. Zaelzer, and G. Vargas. 2007. ThermoTRP channels as modular proteins with allosteric gating. *Cell Calcium.* 42:427–438. <https://doi.org/10.1016/j.ceca.2007.04.004>
- Lee, B.H., and J. Zheng. 2015. Proton block of proton-activated TRPV1 current. *J. Gen. Physiol.* 146:147–159. <https://doi.org/10.1085/jgp.201511386>
- Lin, Z., Q. Chen, M. Lee, X. Cao, J. Zhang, D. Ma, L. Chen, X. Hu, H. Wang, X. Wang, et al. 2012. Exome sequencing reveals mutations in TRPV3 as a cause of Olmsted syndrome. *Am. J. Hum. Genet.* 90:558–564. <https://doi.org/10.1016/j.ajhg.2012.02.006>
- Liu, B., J. Yao, Y. Wang, H. Li, and F. Qin. 2009. Proton inhibition of unitary currents of vanilloid receptors. *J. Gen. Physiol.* 134:243–258. <https://doi.org/10.1085/jgp.200910255>
- Liu, B., J. Yao, M.X. Zhu, and F. Qin. 2011. Hysteresis of gating underlines sensitization of TRPV3 channels. *J. Gen. Physiol.* 138:509–520. <https://doi.org/10.1085/jgp.201110689>
- Luo, J., R. Stewart, R. Berdeaux, and H. Hu. 2012. Tonic inhibition of TRPV3 by Mg²⁺ in mouse epidermal keratinocytes. *J. Invest. Dermatol.* 132:2158–2165. <https://doi.org/10.1038/jid.2012.144>
- Macikova, L., L. Vyklicka, I. Barvik, A.I. Sobolevsky, and V. Vlachova. 2019. Cytoplasmic Inter-Subunit Interface Controls Use-Dependence of Thermal Activation of TRPV3 Channel. *Int. J. Mol. Sci.* 20:3990. <https://doi.org/10.3390/ijms20163990>
- Miller, M., M. Wu, J. Xu, D. Weaver, M. Li, and M.X. Zhu. 2011. High-Throughput Screening of TRPC Channel Ligands Using Cell-Based Assays. In *TRP Channels*. M.X. Zhu, editor. CRC Press/Taylor & Francis, Boca Raton, FL. 1–20.
- Ohman, H., and A. Vahlquist. 1994. In vivo studies concerning a pH gradient in human stratum corneum and upper epidermis. *Acta Derm. Venereol.* 74:375–379. <https://doi.org/10.2340/0001555574375379>
- Peier, A.M., A.J. Reeve, D.A. Andersson, A. Moqrich, T.J. Earley, A.C. Hergarden, G.M. Story, S. Colley, J.B. Hogenesch, P. McIntyre, et al. 2002. A heat-sensitive TRP channel expressed in keratinocytes. *Science.* 296:2046–2049. <https://doi.org/10.1126/science.1073140>
- Ryu, S., B. Liu, J. Yao, Q. Fu, and F. Qin. 2007. Uncoupling proton activation of vanilloid receptor TRPV1. *J. Neurosci.* 27:12797–12807. <https://doi.org/10.1523/JNEUROSCI.2324-07.2007>
- Shaw, D.E. 2005. A fast, scalable method for the parallel evaluation of distance-limited pairwise particle interactions. *J. Comput. Chem.* 26:1318–1328. <https://doi.org/10.1002/jcc.20267>
- Shimada, H., T. Kusakizako, T.H. Dung Nguyen, T. Nishizawa, T. Hino, M. Tominaga, and O. Nureki. 2020. The structure of lipid nanodisc-reconstituted TRPV3 reveals the gating mechanism. *Nat. Struct. Mol. Biol.* 27:645–652. <https://doi.org/10.1038/s41594-020-0439-z>
- Singh, A.K., L.L. McGoldrick, and A.I. Sobolevsky. 2018. Structure and gating mechanism of the transient receptor potential channel TRPV3. *Nat. Struct. Mol. Biol.* 25:805–813. <https://doi.org/10.1038/s41594-018-0108-7>
- Singh, A.K., L.L. McGoldrick, L. Demirkhanyan, M. Leslie, E. Zakharian, and A.I. Sobolevsky. 2019. Structural basis of temperature sensation by the TRP channel TRPV3. *Nat. Struct. Mol. Biol.* 26:994–998. <https://doi.org/10.1038/s41594-019-0318-7>
- Smith, G.D., M.J. Gunthorpe, R.E. Kelsell, P.D. Hayes, P. Reilly, P. Facer, J.E. Wright, J.C. Jerman, J.P. Walhin, L. Ooi, et al. 2002. TRPV3 is a temperature-sensitive vanilloid receptor-like protein. *Nature.* 418:186–190. <https://doi.org/10.1038/nature00894>
- Szöllösi, A.G., N. Vasas, Á. Angyal, K. Kistamás, P.P. Nánási, J. Mihály, G. Béke, E. Herczeg-Lisztes, A. Szegedi, N. Kawada, et al. 2018. Activation of TRPV3 Regulates Inflammatory Actions of Human Epidermal Keratinocytes. *J. Invest. Dermatol.* 138:365–374. <https://doi.org/10.1016/j.jid.2017.07.852>
- Taggart, M.J., and S. Wray. 1998. Hypoxia and smooth muscle function: key regulatory events during metabolic stress. *J. Physiol.* 509:315–325. <https://doi.org/10.1111/j.1469-7793.1998.315bn.x>
- Tominaga, M., M.J. Caterina, A.B. Malmberg, T.A. Rosen, H. Gilbert, K. Skinner, B.E. Raumann, A.I. Basbaum, and D. Julius. 1998. The cloned capsaicin receptor integrates multiple pain-producing stimuli. *Neuron.* 21:531–543. [https://doi.org/10.1016/S0896-6273\(00\)80564-4](https://doi.org/10.1016/S0896-6273(00)80564-4)
- Wakabayashi, M., T. Yoshioka, K. Higashino, Y. Numata, Y. Igarashi, and A. Kihara. 2017. Decreases in 15-lipoxygenase metabolites in Olmsted syndrome model rats. *J. Dermatol. Sci.* 85:186–196. <https://doi.org/10.1016/j.jdermsci.2016.12.013>
- Waldmann, R., and M. Lazdunski. 1998. H⁽⁺⁾-gated cation channels: neuronal acid sensors in the NaC/DEG family of ion channels. *Curr. Opin. Neurobiol.* 8:418–424. [https://doi.org/10.1016/S0959-4388\(98\)80070-6](https://doi.org/10.1016/S0959-4388(98)80070-6)
- Wang, Y.Z., and T.L. Xu. 2011. Acidosis, acid-sensing ion channels, and neuronal cell death. *Mol. Neurobiol.* 44:350–358. <https://doi.org/10.1007/s12035-011-8204-2>
- Wang, J., Y. Wang, W.W. Cui, Y. Huang, Y. Yang, Y. Liu, W.S. Zhao, X.Y. Cheng, W.S. Sun, P. Cao, et al. 2018. Druggable negative allosteric site of P2X3 receptors. *Proc. Natl. Acad. Sci. USA.* 115:4939–4944. <https://doi.org/10.1073/pnas.1800907115>
- Wang, J., H. Li, C. Xue, H. Chen, Y. Xue, F. Zhao, M.X. Zhu, and Z. Cao. 2020. TRPV3 enhances skin keratinocyte proliferation through EGFR-dependent signaling pathways. *Cell Biol. Toxicol.* 2020:13. <https://doi.org/10.1007/s10565-020-09536-2>
- Wilson, N.J., C. Cole, L.M. Milstone, A.E. Kiszewski, C.D. Hansen, E.A. O'Toole, M.E. Schwartz, W.H. Irwin McLean, and F.J.D. Smith. 2015. Expanding the Phenotypic Spectrum of Olmsted Syndrome. *J. Invest. Dermatol.* 135:2879–2883. <https://doi.org/10.1038/jid.2015.217>
- Winter, Z., A. Buhala, F. Ötvös, K. Jósavay, C. Vizler, G. Dombi, G. Szakonyi, and Z. Oláh. 2013. Functionally important amino acid residues in the transient receptor potential vanilloid 1 (TRPV1) ion channel—an overview of the current mutational data. *Mol. Pain.* 9:30. <https://doi.org/10.1186/1744-8069-9-30>
- Xiao, R., J. Tang, C. Wang, C.K. Colton, J. Tian, and M.X. Zhu. 2008b. Calcium plays a central role in the sensitization of TRPV3 channel to repetitive stimulations. *J. Biol. Chem.* 283:6162–6174. <https://doi.org/10.1074/jbc.M706535200>
- Xiao, R., J. Tian, J. Tang, and M.X. Zhu. 2008a. The TRPV3 mutation associated with the hairless phenotype in rodents is constitutively active. *Cell Calcium.* 43:334–343. <https://doi.org/10.1016/j.ceca.2007.06.004>
- Xu, H., I.S. Ramsey, S.A. Kotecha, M.M. Moran, J.A. Chong, D. Lawson, P. Ge, J. Lilly, I. Silos-Santiago, Y. Xie, et al. 2002. TRPV3 is a calcium-permeable temperature-sensitive cation channel. *Nature.* 418:181–186. <https://doi.org/10.1038/nature00882>

- Xu, H., M. Delling, J.C. Jun, and D.E. Clapham. 2006. Oregano, thyme and clove-derived flavors and skin sensitizers activate specific TRP channels. *Nat. Neurosci.* 9:628–635. <https://doi.org/10.1038/nn1692>
- Yan, K., X. Sun, G. Wang, Y. Liu, and K. Wang. 2019. Pharmacological Activation of Thermo-Transient Receptor Potential Vanilloid 3 Channels Inhibits Hair Growth by Inducing Cell Death of Hair Follicle Outer Root Sheath. *J. Pharmacol. Exp. Ther.* 370:299–307. <https://doi.org/10.1124/jpet.119.258087>
- Yoshioka, T., K. Imura, M. Asakawa, M. Suzuki, I. Oshima, T. Hirasawa, T. Sakata, T. Horikawa, and A. Arimura. 2009. Impact of the Gly573Ser substitution in TRPV3 on the development of allergic and pruritic dermatitis in mice. *J. Invest. Dermatol.* 129:714–722. <https://doi.org/10.1038/jid.2008.245>
- Zubcevic, L., M.A. Herzik Jr., M. Wu, W.F. Borschel, M. Hirschi, A.S. Song, G.C. Lander, and S.Y. Lee. 2018. Conformational ensemble of the human TRPV3 ion channel. *Nat. Commun.* 9:4773. <https://doi.org/10.1038/s41467-018-07117-w>
- Zubcevic, L., W.F. Borschel, A.L. Hsu, M.J. Borgnia, and S.Y. Lee. 2019. Regulatory switch at the cytoplasmic interface controls TRPV channel gating. *eLife.* 8:e47746. <https://doi.org/10.7554/eLife.47746>